MODELING MICROWAVE HEATING OF APPLE CYLINDERS USING HYBRID MIXTURE THEORY BASED TRANSPORT EQUATIONS COUPLED WITH MAXWELL'S LAWS OF ELECTROMAGNETISM

BY

JIE DENG

THESIS

Submitted in partial fulfillment of the requirements
for the degree of Master of Science in Food Science and Human Nutrition
with a concentration in Food Science
in the Graduate College of the
University of Illinois at Urbana-Champaign, 2014

Urbana, Illinois

Adviser:

Associate Professor Pawan Singh Takhar

ABSTRACT

To develop an efficient microwave drying scheme for apple cylinders, a multiscale mathematical model was developed to predict the moisture and temperature profiles. Two-scale hybrid mixture theory (HMT) based transport equations were utilized to describe the fluid (water & gas phases) transport during the microwave drying of apple cylinders. Maxwell's electromagnetic equations were coupled with HMT based transport equations to obtain heating source for evaporative moisture loss in the food matrix. A commercial finite element package (COMSOL Multiphysics ver 4.4) was employed to solve these equations in order to obtain the spatial and temporal profiles for moisture and temperature within the sample. The validation experiments were conducted with a domestic microwave oven. The comparison of the moisture profiles obtained through simulations and experiments resulted in an average absolute difference value of 37.9%. For comparison of experimental and predicted temperature values a parametric sweep was performed. The developed model could be employed efficiently for the prediction of the moisture distribution. The temperature change trend could also be predicted using the developed model.

ACKNOWLEDGEMENTS

I would like to express my deep gratitude and thanks to my advisor Dr. Pawan Takhar for his guidance and encouragement throughout my graduate years. He opened the door for me to get access to continue my graduate study in the United States. He helped me with my studies and research with his professional attitude, patience and knowledgeable skills. He led me into a totally new field of mathematical modeling and gave me many valuable suggestions. I experienced the intricacies of modeling because of his guidance.

I am very grateful to my committee members, Dr. Graciela Padua, Dr. Hao Feng and Dr. Kaustubh Bhalerao. They gave me valuable suggestions on my graduation and my paper. I feel proud to join this University and the FSHN department, as faculties and students here are always willing to help with their professional and sincere attitudes.

I was so lucky to enroll in this perfect lab since 2011. Lab mates here helped me a lot not only on my study but also my life. We knew each other in Texas and moved together to Illinois. When I felt helpless here, they are always the one who stand by me. They are my sincere friends and I would like to give my sincere thanks to them.

My special thanks to my parents, my brother and my boyfriend. Their support and encouragement in my life gave me the inspiration and motivation to be a better person.

TABLE OF CONTENTS

1. Introduction

Apple, originating from Central Asia, is a tree fruit that has been widely cultivated for thousands of years. Currently, the global apple production has reached approximately 69 million tons per year with more than 7,500 cultivars. China and the United States are the top apple producing countries, which occupy half production around the world. Various processing methods of apples have been developed in these two countries (*USDA National Nutrient*, 2011).

An apple contains high amount of dietary fiber (2.4g/100g), sugar (10.39g/100g) and various vitamins, which can help to reduce the risk of some cancer and have positive effects in decreasing obesity (*Food and Agriculture Organization of the United States*, 2000). The proverb as "An apple a day, keeps the doctor away" reflects people's recognition of apples' health effects. Earlier mice studies found that apples contain ursolic acid in peels that can increase the skeletal muscle and acetylcholine, which enhances the brain function, speeds up information transmission and delays senescence.

Raw apples are consumed as healthy fruits with different cultivars. Due to the high production of apples, there are more than enough of them for raw consumption. The conservation of large amount of apples becomes a problem due to the high moisture content within the apple, which makes apple an ideal environment for bacteria to propagate. People also demand various apple products, like chips, salad, juice and sauce. These products greatly enhance the consumption, reduce the corruption and satisfy consumers' needs. Thus, drying is necessary for the preservation and new products

development, which stimulates new consumption method of apple, inhibits the growth of bacteria and prevents fruit corruption.

1.1 Drying

Drying of foods is a traditional and widely used method to prevent its spoilage and enhance quality attributes. It is a simultaneous heat and mass transfer process. In the past, solar energy was used to speed up the drying process, which was largely dependent on the weather conditions. A little later, hot air was also utilized to speed up the drying process since it could increase the driving force for the heat transfer.

With the occurrence of new drying technologies, some other assisted methods had been put forward, which included osmotic, vacuum, fluidized bed, nuclear, infrared, nuclear magnetic resonance and microwave oven (Mujumdar, 2004). Among these methods, microwave assisted drying was mostly commonly applied based on its advantages of rapid drying, convenient equipment design, large-scale application and economic considerations.

1.2 Development of Microwave Drying

The microwave oven was invented by Percy Spencer after World War II (Spencer, 1950) and introduced for home use by Tappan in 1955. In 1967, Amana Corporation produced the first countertop microwave oven. After that, there was a broad industrial and domestic microwave oven application, which motivated abundant research in this field.

In the conventional drying method, heat is provided externally and moisture is evaporated out from the inside (Figure 1). In this drying method, the heat is transferred from the source to the food surface and then to the interior, which makes drying a slow process. However, for the microwave drying, the electromagnetic waves can penetrate into the food and interact with the whole sample, thus heat is induced inside the sample, which makes it a rapid drying method (Schiffmann, 2006).

The microwave frequency ranges from 300 MHz to 300 GHz and the wavelength varies from 1mm to 1m. Microwaves are electromagnetic waves, which result from the combination of the electric component and magnetic component, and carry the energy that propagated in the electromagnetic field (Vollmer, 2004; Dibben, 2001). The microwave drying mechanism is based on the interaction between water dipolar molecules and the electromagnetic field, which makes it a selective drying process. Thus, the higher moisture content portion of a product can absorb more energy (Khraisheh, Cooper & Magee, 1997). The parts of the sample with lower moisture are heated more by the conduction method. This drying method helps reducing the overheating of the portion with less moisture content.

1.3 Hybrid Mixture Theory

The model proposed in this study is based on the hybrid mixture theory (HMT), which utilizes mutiscale laws of conservation of mass, momentum, energy and entropy (Singh, Cushman and Maier, 2003). The HMT theory has an advantage that the mesoscale variables can be associated with the microscale counterparts based on the classical mixture

theory (Weinstein, 2005). It averages the equations at microscale to derive equations at higher scales using the up-scaling technique, and formulating constitutive relations and exploiting the entropy inequality at macroscale (Bennethum and Cushman, 1999).

The constitutive equations are formulated at macroscale based on the entropy inequality (Colman and Noll, 1963). During the up scaling process, some microscale information get lost but the microscale transport mechanisms are incorporated (Singh et al., 2003). As the material coefficients are easier to be obtained at macroscale through experiments, it becomes more convenient to upscale first and then derive the constitutive equations. The representative elementary volumes (REV) are used to solve the equations at higher scales, which can help to reduce the computation time greatly (Takhar, 2014).

There are broad applications of HMT in different areas. Bennethum and Cushman (1996) had utilized this theory to describe the thermo mechanical phenomenon within the porous media. Weinstein (2005) used HMT to describe the swelling and shrinkage in drug delivery system. It has been used to derive the fluid transport equations both in saturated and unsaturated food systems (Singh et al., 2003; Takhar, 2014).

We utilize the HMT based fluid transport equations in this study and the apple cylinders were considered as porous biopolymeric material. The underlying physical mechanisms and unsaturated relations developed recently by Takhar (2014) were incorporated in the model to study the microwave drying process.

1.4 COMSOL Multiphysics

COMSOL Multiphysics is a commercial software package that used to compute physical and chemical phenomena since 1986. It started with the Toolbox of MATLAB, and was renamed with FEMLAB and denominated as COMSOL Multiphysics (ver 3.2) in 2005 (COMSOL Release History, 2013). It is composed of a basic module and eight professional modules, which is based on the finite element and used the mathematical method to solve the practical physical problem.

Large amount of pre-defined physical modules, such as fluid flow, heat conduction, mechanics and electromagnetism, have be utilized by users to build model rapidly. It has been used to improve the signal receive ability of mobile phone and can provide more accurate diagnosis for medical equipment. For this study, it can compute with the implemented partial differential equations (PDEs) and microwave heating module to demonstrate the fluid dynamics and electromagnetism phenomena.

1.5 Previous studies on microwave drying

Because of the advantages and rapid development of microwave assisted drying method, many studies were conducted earlier on microwave drying of food.

Ni, Datta and Torrence (1999) proposed a multiphase porous media model for microwave heating of biomaterials based on Darcy's law, mass balance and heat balance equations, and discussed different boundary conditions. They stated that the fluid transport during intensive microwave drying was driven by gas pressure gradient. As they

explained, the internal heating and evaporation caused the internal pressure gradient, which in turn led to the higher amount of moisture loss. Different boundary conditions were discussed in their work according to whether there was water puffing at the surface. This discussion provided experience for the current study in developing moisture flux at the boundary of food sample. Experiments were performed for the validation of the model in their research, which displayed a satisfying fit. They suggested in the conclusion part that the convection term contribution was slight. However, their equations did not incorporate the elastic properties and could not explain and describe the fluid transport behavior accurately at different drying states (glassy, rubbery and glass-transition).

Rakesh and Datta (2011) introduced the deformation model for microwave puffing. They built the model based on conservation of mass, momentum and energy. Convection, conduction, phase change (evaporation) and microwave heating terms were included for the conservation of energy law. In their work, the computational model and physical changes during puffing process were stated specifically, which gave a clear clue for the startup of microwave heating simulation. They suggested that the intensive microwave heating was a favorable and effective method for the success of puffing process, which also exhibited that microwave heating worked efficiently in food drying due to the intensive power supply.

Takhar (2011a) developed the coupled moisture transport and stress equations for the corn kernel drying based on hybrid mixture theory. Because of the volume change during the drying process, the moving mesh was introduced to solve the fluid transport equations by converting the Eulerian coordinates to Lagarangian coordinates through Laplace transformation. This solution method provided an example to solve problems with

moving boundaries. The stress relaxation function was introduced and imported into the fluid transport equations to describe the mechanical properties of corn kernels during drying, which has been applied in current work to evaluate the coefficient of elasticity of apples. In his companion paper, the fluid transport and stress development equations were solved and simulation results were validated by experiment values (Takhar, 2011b). This study provided guidance for the solution scheme, which had been applied in the solution of fluid transport equations for microwave drying.

Pakowski and Adamski (2012) explained the pressure formation mechanism for apple cylinders during drying. The experimental results obtained from their work demonstrated that the shrinkage of apple during drying was caused by the formation of negative pressure within the apple sample. The axial compression test was conducted and the expression of Young's modulus as a function of moisture content for apple was derived, which had been used in current study.

In the theoretical study of microwave heating of apples on the fluidized bed, Chen, Wang and Mujumdar (2001) proposed an efficient scheme for microwave drying. Based on the comparison of drying effects with uniform, sinusoidal and rectangular wave patterns, they concluded that the intermittent heating with rectangular wave pattern improved the drying rate significantly as the sample could absorb more microwave energy under this wave condition. Their modeling results displayed a greater moisture loss and temperature increase in the sample under microwave heating, which proved the microwaves caused the faster drying rate. This study also gave a suggestion in deciding the wave pattern.

Feng, Cavalieri and Plumb (2001) studied the microwave drying of porous materials on a spouted bed and built a model based on the governing equations for heat and mass

transfer. The representative food stuff chosen for the experiments was the hygroscopic porous material, apple. In their work, a mathematical model was proposed by assuming the sample as homogeneous and isotropic. The fluid transport relationship was developed based on the generalized Darcy's law and Fick's law. They considered the bound-water flux caused by chemical potential gradient and took the internal vapor generation into consideration with the assistance of gas-pressure equation. The mass transfer equations for free water, bound water, vapor and air phases and energy balance equation were established for a representative elementary volume (REV). Application of up-scaling method assisted the built of governing equations for their study. Related physical and thermo parameters were discussed in their work for the solution of the model. Numerical analysis and experimental results proved that the microwave and spouted-bed drying was an effective method for drying of porous biomaterials. However, in their study, the microwave power level was low, due to which the drying process took over an hour to complete.

In the microwave drying, it was important to evaluate the uniformity effects of the dried food products. Geedipalli, Rakesh and Datta (2007) built a model to assess if the turntable in microwave cavity could improve the heating uniformity of sample. Their model was built on the Maxwell's equations and heat balance equation. The numerical results obtained through ANSYS software were compared with the experimental values. They concluded that the model could be used to predict the temperature distribution on a rotating carousel efficiently and the temperature uniformity was improved 43% with the rotating turntable in the microwave oven.

Andres, Bilbao and Fito (2004) studied the drying kinetics of apple cylinders under combined hot air and microwave condition. They proposed several combination methods at different air temperature and incident power levels, which included applying the microwave at initial stage, at the start of falling drying rate period and at the last stage. Their experimental results demonstrated that the microwave power level would affect the drying process, which motivated the study of drying effects at different power supply levels in the current work.

Vacuum assisted microwave drying has been studied since the vacuum led to the higher mass transfer due to the increased pressure gradient within the sample. Pere and Rodier (2002) conducted the experiments with water saturated glass beads and pharmaceutical granules to study the internal mass transfer during drying. According to their experimental results, the permeability was the limiting factor at the initial drying stage and there was no obvious effects observed at the following periods. However, the mass transfer at the last drying stage was mainly affected by the electromagnetic energy absorption. This provided some information for the current study that characteristics of different drying stages should be taken into consideration, especially in the intensive microwave drying.

Ayappa (1997) reviewed the modeling of the fluid transport process and discussed different phenomena (resonance, hot spots, edge effects etc.) that occurred during microwave drying. The edge effects and hot spots discussions from Ayappa's study have been taken into consideration in the current study. But for the energy conservation terms, they did not consider the contribution from different phases, which resulted in the inaccurate evaluation of the heat storage and convection terms.

Zhang and Datta (2005) analyzed the microwave concentration in different shapes of food. In the study, they built the mathematical model for lossy dielectric samples and focused on the distribution of electrical fields with plane waves and cavity standing waves. In order to elucidate the microwave concentration (focusing and resonance) within the sample, the heating effects caused by wavelength, dielectric properties, and sample size were discussed. Mathematical formulations proved that wavelength played a significant role in determining the microwave heating concentration. The dielectric properties affected the focusing location, which suggested the variation of heat concentration. These factors have also been taken into consideration in the current study.

All these previous studies provided a clear clue for the current study from different aspects of the development of mathematical model for microwave drying. The current work was based on those studies but provided a more efficient scheme for the modeling of microwave drying. In the current study, the sample was treated as elastic polymers to obtain partial-differential fluid transport equations that could successfully exhibit the effects at all drying states (glassy, rubbery and glass-transition). The fluid transport within the sample was considered as a multiphase porous medium transport, which was built on multiphase flow, binary diffusion and pressure driven flow mechanisms. When coupled with the microwave intensive heating, the heat transfer rate increased and the drying efficiency improved.

2. Microwave Drying Mechanisms and Fundamentals

2.1 Microwave dying mechanism

Microwaves are manifestation of energy resulting from the interaction with dielectric materials, which were apple cylinders in this study. The reason that food can be dehydrated efficiently within the microwave equipment is mainly based on the interaction between water dipolar molecules and the electromagnetic field (Khraisheh, Cooper and Magee, 1997). At high frequencies, the water molecules that place in the microwave electromagnetic field turn around (Dibeen, 2011). Usually, the frequency used in industrial and domestic microwave oven is 2450MHz, which is also the resonance frequency of water molecules (Mudget, 1986). As the water molecules are unable to follow the fast reverse of the electric field, the phasor falls behind the applied electromagnetic field (Metaxas and Meredith, 1983; Vollmer, 2004). Thus, a current component is in the same phase with the field. In this way, the power is absorbed by the dielectric food material (Metaxas and Meredith, 1983). Also, due to collision of ions in food with the ionized water molecules in the electromagnetic field, the induced ordered kinetic energy is transformed to disordered kinetic energy, resulting in the production of heat energy (Schiffmann, 2006). Then, the dielectric material absorbs the electromagnetic energy. The higher moisture content portion of a product can absorb more energy, thus making the microwave drying as a selective drying method. The parts with lower moisture are heated more by the conduction method. This drying method helps reducing the overheating of the portion with less moisture content.

The wave frequency is closely related to the drying effects. When the drying is conducted in the field with high frequency, the penetration depth is very small, which causes the uneven energy distribution that the surface absorbs enough energy while the interior still remains cold. However, if the food is dehydrated at rather low frequency field, the penetration depth into the sample will be large and heat cannot be concentrated. The frequencies that have been applied in industry include 915 MHz and 2450 MHz. The latter frequency is the standard requirement for both domestic and industrial application in the United State since it is also the resonance frequency of water (Mudget, 1986). Due to the typical frequency applied, the electric field produced by the magnetron oscillates 2.45 billion times per second. The oscillation causes the friction between water molecules and the heat is produced (Vollmer, 2004). The water is heated and evaporated out, and the food is dried.

Due to the greater dielectric constant and dielectric loss factor of water compared to the solid materials to be dried, higher moisture content part in the sample absorbed more energy and led to a selective and efficient heating method (Chen et al., 2001). As the food sample can absorb microwave energy directly and heat is produced internally, the microwave drying is a volumetric heating method with faster drying rate (Pere and Rodier, 2002).

2.2 Principles of Operation

The magnetron in the oven produces microwaves, which are fed into the resonant cavity through waveguide (Vollmer, 2004). The magnetron is a “cross-field” device, which

is composed of anode, cathode, coupling loop and resonating cavity. The anode is made of a metal with high conductivity like oxygen-free copper. It works together with the cathode to provide the space for the interaction between electrons and high frequency electromagnetic field (Metaxas and Meredith, 1983). The cathode is the heart of the vacuum tube. A magnetic field parallel to the filament is imposed through a permanent magnet. When the power is supplied, the electrons are stimulated and the existing magnetic field causes the ejection of electrons from the cathode (Metaxas and Meredith, 1983). The electrons follow a radial pathway and the magnetic field exerts force on these charges. The electrons tend to sweep around the circle of the resonating cavity, which are open cylindrical cavities around the rim of the chamber (Figure 2). As there are excessive negative charges where electrons sweep by, the charges tend to be pulled back. The pulled back and forth motion leads to the oscillation of electrons and impart energy into the cavity, which results in the production of electromagnetic waves (Vollmer, 2004). Part of the produced power is extracted with a short antenna that connects to the waveguide.

Waveguide is a hollow conductive pipe that can carry the high frequency microwaves with much less power loss (IEEE standard dictionary of electrical and electronics terms, 1996). In an open space, the microwaves propagate in different directions and power loss is proportionally to the square of the distance. In the waveguide, the waves are confined to propagate in one direction with no power loss in ideal conditions. Thus, waveguide is a perfect medium that can perform the function to carry the microwaves into the chamber.

2.3 Objective of this study

The objective of this study was to develop a mathematical model built on multiscale fluid transport equations, heat balance and electromagnetic wave equations to describe the moisture loss and temperature increase of the sample during the microwave drying process. Generalized Darcy's law was utilized to describe the fluid flow in porous structure; generalized energy balance equation of de Vries (1958) was used to explain the heat transfer process and Maxwell's equations were applied to determine the electromagnetic heat dissipation in the sample. These theories were incorporated together into this model in order to obtain an efficient scheme to describe the microwave drying process. The obtained temporal and spatial results of moisture content and temperature were compared with the experimental values to validate the model.

3. Model Development

3.1 Assumptions

To develop the multiscale fluid transport equations, the following assumptions were made:

- Solid, water and gas phases are continuous; the solid phase and water phase are incompressible at microscale;
- The food sample in this study is homogeneous and isotropic;
- Gravity effects can be neglected since they have little impact compared to the fluid flow caused by the pressure gradient;
- The electromagnetic field is distributed uniformly within the sample

3.2 Mass Balance Equation

During the microwave drying process, the moisture moves toward surface in liquid and vapor forms. The water and gas phases follow the mass conservation law. The mass balance equation for the α phase can be written as (Achanta and Cushman1994):

$$\frac{D^{\alpha}(\varepsilon^{\alpha}\rho^{\alpha})}{Dt}+\varepsilon^{\alpha}\rho^{\alpha}\nabla\cdot\boldsymbol{v}^{\alpha}=\sum_{\substack{\beta=w,g\\ \beta\neq a}}{}^{\beta}\hat{e}^{\alpha}\quad,\quad \text{where } \alpha=\text{w, g} \tag{1}$$

Where $\frac{D^{\alpha}}{Dt}$ is the material time derivative with respect to the α phase, $\sum_{\substack{\beta=w,g\\ \beta\neq a}}{}^{\beta}\hat{e}^{\alpha}$ is the evaporation term, which determines the mass gain or loss rate of gas from the water phase due to expansion of condensation.

If we convert material time derivative and velocity of (1) to the one with respect to the solid phase, then it is deducted as (Takhar, 2014):

$$\frac{D^s(\varepsilon^\alpha \rho^\alpha)}{Dt} + \nabla \cdot (\varepsilon^\alpha \rho^\alpha \boldsymbol{v}^{\alpha,s}) - \frac{\dot{\varepsilon}^s}{\varepsilon^s} \varepsilon^\alpha \rho^\alpha = \sum_{\substack{\beta=w,g \\ \beta \neq a}} {}^{\beta}\hat{e}^{\alpha} \text{, where } \alpha\text{=w, g} \tag{2}$$

Based on the relation $\sum_{\alpha=s,w,\mathrm{g}} \varepsilon^\alpha = 1$ and $\sum_{\alpha=s,w,g} \dot{\varepsilon}^\alpha = 0$, the volume fraction of solid is expressed as $\varepsilon^s = 1 - \varepsilon^w - \varepsilon^g$ and the material derivative of the solid phase is $\dot{\varepsilon}^s = -(\dot{\varepsilon}^w + \dot{\varepsilon}^g)$.

By assuming the water as incompressible at macroscale, we obtain

$$\frac{D^s \rho^w}{Dt} = 0 \tag{3}$$

Using (2) and (3), the mass balance equation for water phase can be expressed as:

$$\frac{D^s \varepsilon^w}{Dt} + \nabla \cdot (\varepsilon^w \boldsymbol{v}^{w,s}) - \varepsilon^w \frac{\dot{\varepsilon}^s}{\varepsilon^s} = -\frac{{}^{w}\hat{e}^{g}}{\rho^w} \tag{4}$$

Because of the compressibility of the gas phase (air-vapor mixture) $\frac{D^s \rho^g}{Dt} \neq 0$. The mass balance equations for gas phase can be written as:

$$\frac{D^s(\varepsilon^g \rho^g)}{Dt} + \nabla \cdot (\varepsilon^g \rho^g \boldsymbol{v}^{g,s}) - \frac{\dot{\varepsilon}^s}{\varepsilon^s} \varepsilon^g \rho^g = {}^{w}\hat{e}^{g} \tag{5}$$

Eqs. (4) and (5) are the mass balance equations for water and gas phases, which are applied together to describe the fluid transport during the microwave drying process of apple cylinders in this study.

To derive the expression for the rate of evaporation, the near-equilibrium relationship of Gibbs free energy based relation between the water and vapor phases (Takhar, 2014; Fang and Ward, 1999) were used.

$$ {}^{w}\hat{e}^{g} = \frac{RT}{\xi^{v}} \ln\left(\frac{p^{w}}{p^{v}}\right) \tag{6} $$

Where R is the specific gas constant for water vapors ($\mathrm{J/kg \cdot K}$), ξ^{v} is the near-equilibrium evaporation rate coefficient (1/s), p^{w} is the vapor pressure of liquid water in a pore and p^{v} is the bulk vapor pressure of water in the gas phase in the pore.

3.3 Generalized Darcy's law

During the microwave drying process, the internal heating increases the pressure gradients, which in turn enhances the fluid transport process. This pressure driven flow is the dominant mechanism in microwave drying and can be explained by Darcy's law (Ni, Datta and Torrance, 1999). Usually, the Darcy's law is combined with other laws to obtain an accurate description for fluid flow in porous material. In this study, the generalized Darcy's law developed by Takhar (2014) is employed to describe the fluid transport.

As the water is assumed to be flowing slowly and the gravity effects can be neglected, the generalized Darcy's law for the water phase is expressed as (Takhar, 2014):

$$ \boldsymbol{v}^{w,s} = -\left[\frac{K^{w}}{\mu^{w}} \varepsilon^{w} \nabla p^{w} + \varepsilon^{w} D^{w} \nabla \varepsilon^{w} + \varepsilon^{w} \frac{K^{w}}{\mu^{w}} N^{w} \nabla \dot{\varepsilon}^{w}\right] \tag{7} $$

The first term on the right side is the pressure gradient term of Darcy's law; the second term incorporates the flow caused by fluid concentration gradient and the last term includes the viscous resistance of the polymeric matrix to the fluid flow (Achanta, Okos and Cushman1997; Takhar, 2014);.

For the velocity of gas phase with respect to the solid, the generalized Darcy's law can be simplified as (Takhar, 2014):

$$\boldsymbol{v}^{g,s} = -\frac{K^g}{\mu^g}\varepsilon^g \nabla p^g \tag{8}$$

Based on the binary diffusion theory, Fick's law is used to derive the velocity of vapor phase relative to the gas as follows (Bird, Stewart & Lightfoot, 2006):

$$\boldsymbol{v}^{v,g} = -D^v \frac{\nabla \omega^v}{\omega^v} \tag{9}$$

Where $\omega^v = \frac{\rho^v}{\rho^g}$ is the mass fraction of vapor phase. The relative velocity of vapor with respect to solid can be expressed as:

$$\boldsymbol{v}^{v,s} = \boldsymbol{v}^{v,g} + \boldsymbol{v}^{g,s} \tag{10}$$

Thus, the velocity expression of water and gas phases with respect to the solid phase is derived from the generalized Darcy's law. They are incorporated into the mass balance equations to obtain the generalized fluid transport equations for each phase.

3.4 Electromagnetic wave equations

Microwaves are electromagnetic waves that generated by magnetrons and fed into the resonant cavity through the waveguide (Vollmer, 2004). Microwaves interact with dielectric materials to generate heat energy.

The Maxwell's equations are used to explain how the electric and magnetic fields are generated and altered by charges and currents, which are composed of four basic laws (Fuller, 1990).

$$\nabla \cdot \boldsymbol{D} = \rho \tag{11}$$

$$\nabla \cdot \boldsymbol{B} = 0 \tag{12}$$

$$\nabla \times \boldsymbol{H} = \boldsymbol{J} + \frac{\partial \boldsymbol{D}}{\partial t} \tag{13}$$

$$\nabla \times \boldsymbol{E} = -\frac{\partial \boldsymbol{B}}{\partial t} \tag{14}$$

Where $\boldsymbol{D}$ is the electric flux density (C/m^2), ρ is the charge density (C/m^3), $\boldsymbol{B}$ is the magnetic flux density (Tesla), $\boldsymbol{H}$ is the magnetic field intensity (A/m), $\boldsymbol{J}$ is the current density (A/m^2) and $\boldsymbol{E}$ is the electric field intensity (V/m).

The first law is the Gauss' theorem for electricity, which describes that the electric flux density vector out of a closed surface is equal to the total free charges enclosed by it. The second law is the Gauss' theorem for magnetism, which denotes that magnetic flux density out of a closed surface is zero. The third law is the Ampere's law, which states that the line integral of the magnetic field around a closed path is equal to the total current flux

through a surface bounded by that path. The fourth law is the Farady's law of electromagnetic induction, which illustrates that the line integral of the electric field around a closed path is equal to the rate of change of the magnetic flux through a surface bounded by that path (Fuller, 1990).

The flux density is linearly related to the field intensity as follows:

$$\boldsymbol{B} = \mu \boldsymbol{H} \tag{15}$$

$$\boldsymbol{D} = \varepsilon \boldsymbol{E} \tag{16}$$

Where μ is the permeability (H/m) and ε is the permittivity (F/m).

Solution of Maxwell's equations gives the electromagnetic wave equation:

$$\nabla \times \mu_r^{-1}(\nabla \times \boldsymbol{E}) - k_0^2(\varepsilon_r - \frac{j\sigma}{\omega\varepsilon_0})\boldsymbol{E} = 0 \tag{17}$$

The microwaves heat food volumetrically and the produced power is absorbed by the dielectric material. The microwave energy is distributed in the medium and material, which can be accounted as resistive heat energy and magnetic loss (Wentworth, 2005).

$$Q_m = Q_{rh} + Q_{ml} \tag{18}$$

Where Q_{rh} is the resistive heat energy and Q_{ml} is the magnetic loss.

The resistive heat energy absorbed by the sample can be expressed as:

$$Q_{rh} = \frac{1}{2}\mathrm{Re}(\boldsymbol{J} \cdot \boldsymbol{E}^*) \tag{19}$$

The magnetic loss is accounted as:

$$Q_{ml} = \frac{1}{2}\mathrm{Re}(j\omega \boldsymbol{B} \cdot \boldsymbol{H}^{*}) \tag{20}$$

These two parts are combined together to decide the energy absorbed by the food sample. The magnetic loss is usually much less than the resistive loss for the dielectric food materials (foods are not considered as magnetic materials), which can be accounted as zero in this study.

3.5 Energy Conservation Equation

The energy conservation law is based on the conservation of sensible heat, latent heat and microwave power. Thus, the energy conservation equation is described as follows (de Vries, 1958).

$$\sum_{\alpha=w,g,s} \varepsilon^{\alpha}\rho^{\alpha}C_p^{\alpha}\frac{\partial T}{\partial t} + \nabla\cdot[\sum_{\alpha=w,g,s} -\varepsilon^{\alpha}K^{\alpha}\nabla T] + \sum_{\alpha=w,g} \rho^{\alpha}C_p^{\alpha}\nabla T\cdot \boldsymbol{v}_l^{\alpha,s} = -\lambda^{w}\hat{e}^{g} + Q_m \tag{21}$$

The first term on the left side of the equation is the heat storage term, and the second one is the heat conduction term, the third term reflects the heat convection process. On the right hand side of the equation, the first term represents the energy loss due to evaporation and Q_m is the heat source term provided by the electromagnetic field.

3.6 Initial and Boundary Conditions

Based on the assumption that the moisture is distributed uniformly within the sample, the initial volume fraction of water phase is determined from the moisture content on mass dry basis (Eq. 32). The initial volume fraction of gas phase is estimated to be 0.05. The vapor density is calculated using the $p-T$ relation based on the ideal gas law. Initially, the temperature and pressure are assumed to be at equilibrium with the ambient conditions.

At the boundary, there are exchanges of water, gas and heat energy. During the drying process, liquid water moves out of the boundary and the vapor film is superimposed on the surface. (Figure 3). The pressure difference across the film is applied as driving force in the expression of water flux and vapor flux. Neumann boundary conditions are employed to solve the fluid transport equations as shown in Table 1.

As the microwave oven wall is made of stainless steel, the resistive losses are small and the field can only penetrate a short distance outside of the boundary. The impedance boundary conditions (IBC) take this effect into consideration and it can be expressed with the following equation (Senior, 1960):

$$\sqrt{\frac{\mu_0\mu_r}{\varepsilon_0\varepsilon_r - j\frac{\sigma}{\omega}}}\boldsymbol{n}\times\boldsymbol{H}+\boldsymbol{E}-(\boldsymbol{n}\cdot\boldsymbol{E})\boldsymbol{n}=(\boldsymbol{n}\cdot\boldsymbol{E}_s)\boldsymbol{n}-\boldsymbol{E}_s \tag{22}$$

The symmetry boundary of the geometry is treated as a perfect magnetic conductor, which is expressed mathematically as:

$$\boldsymbol{n}\times\boldsymbol{H}=0 \tag{23}$$

The numerical values or relations for various initial and boundary conditions are listed in Table 1 and they are employed together in the COMSOL Multiphysics (Ver. 4.4) to solve the equations.

3.7 Factors affecting the drying process

3.7.1 Dielectric properties of material

The microwave drying is affected by the dielectric properties of the material. Earlier studies have shown that the dielectric properties change with the moisture content and the temperature during the drying process.

Initially, most of the water exists in apple as free water. According to Ryynanen (1995), water is the major polar solvent in food products and re-orients according to the field polarity change. In this way, water plays the major role in determining the dielectric properties of the food sample (Mudget, 1986). Feng Tang and Cavalieri (2002) conducted the dielectric relaxation spectrum (DRS) analysis to state how the moisture content and temperature affect the dielectric properties of apple. The dielectric constant reflects the energy storage ability while the dielectric loss factor includes the dipole loss and ionic loss. Dipole loss is caused when the water dipoles rotate and ionic loss results from the ions migration (Tang, 2005). These two parts are the primary elements of dielectric losses and explain the different dielectric behavior during drying. Initially, due to the high moisture content within the sample, the water dispersion and ionic conduction play the main function; as the moisture content decreases to the medium level, ionic conduction becomes

the primary dominant factor; at the last stage of drying, free water has been removed and only bound water is considered for the water dispersion effect (Feng et al., 2002; Duan, Ren and Zhu, 2012). From their experiments and model, the dielectric loss constant is derived mathematically as (Feng, Tang and Cavalieri., 2001):

$$\varepsilon'' = -23.5999 + 0.158233 \cdot T - 0.000256978 \cdot T^2 - 1.87998 \cdot M + 0.00768435 \cdot M \cdot T \\ \text{-5.6363e-6} \cdot M \cdot T^2 + 0.0289568 \cdot M^2 - 7.66337e-5 \cdot M^2 \cdot T - 4.09947e-5 \cdot M^3 \quad (24)$$

3.7.2 Moisture Diffusivity

Moisture diffusivity is a parameter to evaluate the moisture diffusion ability of the sample. This parameter is important in evaluating the drying effects and it is dependent on the temperature, moisture content and composition structure (Feng et al., 2000). For apple, the effective moisture diffusivity is mainly dependent on the temperature, which can be described with the Arrhenius equation as follows (Schoeber, 1976):

$$D_w = D_0 \exp(-\frac{E_D}{RT}) \quad (25)$$

Where D_0 = constant (m^2/s), E_D = activation energy (kJ/mol)

Based on the experimental analysis conducted by Feng et al. (2000), for apples D_0 equals to 1.56e-6 m^2/s and E_D is 6362.4 kJ/mol.

3.7.3 Mass Transfer Coefficient

The mass transfer coefficient is a needed to calculate the moisture flux on the surface of foods during drying. It is closely related to the moisture content, food properties, geometry and fluid transport velocity. Sherwood number is the ratio of convective mass transfer coefficient and diffusive mass transfer coefficient, which can be used to derive the mass transfer coefficient (Perry and Green, 2008).

$$Sh = 0.3 + [0.62\,\mathrm{Re}^{1/2}\,Sc^{1/3}[1+(\frac{0.4}{Sc})^{2/3}]^{1/4}][1+(\frac{\mathrm{Re}}{282,000})^{5/8}]^{4/5} \quad (26)$$

Where: $\mathrm{Re} = \frac{Lv\rho_g}{\mu_g}$ is the Reynolds number

$Sc = \frac{\mu_g}{\rho_g D_{wg}}$ is the Schmidt number

Therefore, the relationship between Sherwood number and the mass transfer coefficient can be developed as (Perry and Green, 2008):

$$Sh = \frac{h_m RTL}{M_w D_{wg}} \quad (27)$$

With Equation (26) and (27), the mass transfer coefficient can be derived. The volume transfer coefficient of water and gas phases can be derived through the relations $h_w = \frac{h_m}{\rho_w}$ and $h_v = \frac{h_m}{\rho_v}$.

The mass transfer coefficient is critical in assigning the boundary conditions, such as the water flux and vapor flux across the food sample boundary.

3.7.4 Permeability

In the intensive microwave drying, the pressure driven force is the dominant mechanism for the fluid transport (Feng et al., 2000). Permeability is a parameter that defines the ability of the fluid to move through a porous media, which is greatly affected by the pressure gradient within the sample. The relationship between permeability and pressure gradient can be established through Darcy's law. Based on this, Feng et al. (2004) conducted experiments to derive the expression for intrinsic permeability and relative permeability within the porous sample.

The Kozeny-Carman model was used to derive the intrinsic permeability of apple tissue (Feng et al., 2004):

$$K_i = 5.578e-12\frac{\phi^3}{(1-\phi)^2} \tag{28}$$

An empirical relationship was used to develop the relative permeability for gas phase and liquid phase (Feng et al., 2004):

$$k_g = 1.01\exp(-10.86S_w) \tag{29}$$

$$k_l = S_w^3 \tag{30}$$

Where: $S_w = \frac{w}{\phi}$ is the water saturation.

3.7.5 Mechanical properties

The Maxwell rheological model is applied to describe the elastic properties of apple cylinders. During the drying process, the formation of pressure within the solid matrix causes the stress and results in the shrinkage of the sample. The Young's modulus is the parameter to describe the modulus of elasticity of apple sample.

Based on the compression test results, Pakowski and Adamski (2012) derived the expression for Young's modulus for apple sample tissues, which is mainly dependent on the moisture content.

$$E_M = 1.678\times10^6 \cdot \exp(-3.692M) + 0.2277\times10^6 \cdot \exp(-0.1655M) \quad (31)$$

This term is incorporated into the fluid transport equations to derive an accurate description of the drying process..

3.8 Model Implementation

To build the model, governing equations, and initial and boundary conditions were implemented into a commercial finite elements package (COMSOL Multiphysics, Ver 4.4, Burlington, MA). In the model geometry, the microwave oven cavity was connected to a microwave source with a frequency of 2450 MHz. The apple cylinder (2cm diameter ×2cm

depth) was placed at the top center of a cylindrical glass plate. Half of the geometry was simulated due to its symmetric shape, which helped to reduce the solution time.

The frequency-transient study type was selected for this model, which could be used to compute the fluid distribution and temperature change over time together with the electromagnetic field distribution in the frequency domain. The selection of study time step is critical for the computation accuracy. Smaller time steps lead to the better accuacy and stability, but higher computation costs at the same time. The study time step selected for this study was 1s, which could allow at least 2 or 3 orders of magnitude in every time step. Free tetrahedral shape was selected as the mesh elements. The complete mesh included 48571 domain elements, 5128 boundary elements, and 390 edge elements (Figure 4). The model was solved using MUMPS solver with a relative tolerance of 0.01 and an absolute tolerance of 0.001.

4. Experiments

4.1 Experimental equipment

4.1.1 Microwave Oven

The Panasonic NN-CD989S microwave/convection oven (Panasonic Corporation, Osaka Perfecture, Japan) with a maximum power supply level of 1100 Watts was used for the microwave drying experiments (Figure 5). The power levels in this microwave oven can be controlled at 10 different levels, which include 100%, 90%, 80%, 70%, 60%, 50%, 40%, 30%, 20%, 10% of the maximum power supply. Inverter technology is incorporated into this microwave oven. Compared with traditional microwave ovens, this inverter microwave oven can provide constant steady power and allows for different temperature settings.

The cavity dimensions of the microwave are 242mm×412mm×426mm. The cavity capacity is 1.5 cubic feet. There is a turntable ceramic plate for uniform heating purpose. For the application of the fiber optic sensor, the turntable plate was replaced by a still glass plate to evade the twist of sensor wires caused by the turning behavior.

In order to implement the fiber optic sensor within the microwave cavity, the inner structure of the microwave oven was checked and a small hole (smaller than the mesh wire size on the oven door) was drilled on the left side of the oven to avoid the damage of any electrical or heating elements of the oven.

4.1.2 Fiber optic sensor

The temperature within the sample was measured with the fiber optic sensor FOT-L-NS-852B (Fiso technologies, Quebec, Canada) (Figure 6). The temperature sensor can measure temperature from -10℃ to 150℃, which satisfies the temperature requirement for this drying process. The peek tip length of the sensor is 30±1mm with a diameter of 0.8mm (Figure 7). The peek tip of the sensor is hermetic, which can provide stable, accurate and reliable measurements even under the microwave environment and other harsh conditions.

As shown in Figure 8, the peek tip was inserted into the center of the sample with a previously made hole. The ST connector on the sensor is an essential part to connect the fiber optic sensor and the signal conditioner. There is a sensitive zone at the tip, which is the principal part to measure the temperature within the sample. The measured temperature values are based on the line-averaged temperature readings from 5 to 6 mm away from the sensor tip.

4.1.3 Moisture analyzer

In order to decide the moisture loss of the sample during drying, the moisture analyzer was used for rapid determination of moisture content. The OHAUS MB35 moisture analyzer (OHAUS Corporation, Parsippany, NJ) was used for weighing and moisture determination (Figure 9). The halogen lamp is used for even heating with an operating temperature range from 50 ℃ to160℃. The maximum sample capacity 35 g, and the readability is 0.002g with the repeatability of 0.02%.

4.2 Material and Methods

4.2.1 Preparation of sample

Fresh Fuji apples with uniform shape, and without scars were purchased from a local grocery store and stored in the refrigerator at 4 ℃. Before each experiment, the apples were taken out and kept under the room conditions overnight. Apples were cut into cylinders with 2cm diameter and 2cm height and tested in the microwave oven immediately before the onset of oxidation and browning.

4.2.2 Calibration

For the calibration of the moisture content obtained from moisture analyzer, the hot air convection oven method was employed for the moisture content determination of sample at different drying intervals (AOAC, 1990). Samples were dried in the microwave oven cavity for 0min, 0.5min, 1min, 2min, 5min and 8min separately, and weighed with an electronic balance. Three replications were conducted for each drying time interval. Samples were placed in the small open aluminum pans and placed in the air convection oven for drying at 105℃ for 24 hours. The pans with dried samples were taken out and placed in the desiccator to cool down until they reached the room temperature. This cooling down procedure prevented the sample from absorbing moisture from the atmosphere. As the sample cooled down, the electronic balance was employed to weigh the sample. The weight loss reflected the moisture loss during microwave drying at different time intervals.

The moisture analyzer was used for rapid moisture content determination. Prepared samples were dried in the microwave oven for different time intervals (0min, 0.5 min, 1min, 2 min, 5min and 8min). The dried sample were frozen quickly with liquid nitrogen and then grinded into powder with the electronic grinder. Around 0.6 grams grinded powder were spread evenly on the aluminum pan of the moisture analyzer. The halogen element heated the sample to 105 ℃ in less than one minute. Moisture content on wet basis was displayed on the screen and recorded. The moisture content values obtained by moisture analyzer were converted to the oven based values using the calibration curve shown in Figure 11.

4.3 Experimental procedure

The measuring procedure of the moisture content using moisture analyzer was same as mentioned in the calibration process. The sample was placed in the center of the glass plate. The probe of the fiber optic sensor was implemented along the z-axis of the apple cylinder to measure the temperature at center (Figure 7). As soon as the drying started, the graphic acquisition process initiated at the same time and the temperature values within the apple sample were recorded. The studied drying intervals included 0.5min, 1min, 1.5min, 2min, 2.5min, 3min, 3.5min, 4min and 5min. The flow chart of this drying process is shown in Figure 12. The power supply level selected for the drying is 550W.

The fax paper was used to record the microwaves condition inside the oven. Hollow tube was made and placed on the glass plate and heated for 1min. The heating

concentration and waves were displayed in Figure 13(a)-(b). It is evident that the waves have been recorded with around 2cm crest and heating concentrated more at the bottom parts of the tube. The fax paper was placed horizontally with 5cm above the bottom inside the cavity to record the hot spots, which had been demonstrated in Figure 13 (c).

To study the power absorption efficiency, experiments on microwave heating of pure water were conducted at different power supply levels. Glass container filled with pure water ((V_{water} =118cm^3) was placed at the center of the oven cavity. Fiber optic sensor was used to measure the temperature change of the water during the heating process. The temperature values were recorded and had been used to calculate the power absorbed by water using the relation: $Q_a = mC_p \nabla T$.

The experimental data was recorded and imported into Microsoft Excel (Microsoft Inc, Redmond, WA) and Origin 9.1 (OriginLab Corporation, Northampton, MA) for the graph plotting and statistical analysis.

5. Results and Discussion

5.1 Moisture content

The moisture content (g/g solids) of the sample decreased gradually as the drying proceeded. The moisture values obtained through simulations at different spatial locations within the apple cylinders were averaged on volume basis using $M_{avg} = \frac{\int M dV}{\int dV}$. Comparison of the experimental and predicted average moisture content profiles was plotted (Figure 14). At 550W, there was a good agreement of the moisture content between experimental results and simulation values as indicated by the average absolute difference value of 38.29% ($1/n \sum_{i}^{n} \frac{\left| M_{pre.i} - M_{\exp.i} \right|}{M_{\exp.i}}$). This indicated that the model performed well in predicting the moisture change during the microwave drying process. Thus, the model described the fluid transport mechanism effectively.

The initial moisture content ($M_i = 5.887$) was assumed to be distributed uniformly within the sample. The moisture distribution within the sample at 30s, 60s and 120s drying are shown in the slice plots at x-y plane (Figure 15). As shown in these plots, the core of the sample has slightly higher moisture content as compared to other parts (Figure 15a-c). At the top and edge parts of the sample, the moisture content values are slightly lower. This effect is expected to have been caused by: the relative position of the sample and the port (port was located at the right upper side of the sample); the small sample size, which limited the power absorption.

In order to study how does the moisture content change along the sample radius, the spatial distribution of relative moisture content with respect to the values at the center along the radial vector from center to surface of the cylinder were plotted at the center line 16a, 5mm above the center line (Figure 16b), 5mm below the center line (Figure 16c). The moisture content values at the center point were plotted in Figures 16a-c (1). At the center line, the relative moisture content is slightly lower near the surface than that at the core during the drying process, which is caused by the rapid removal of free water near the surface. Above the center line, the relative moisture content values are also slightly lower along the radius than at the center, but they distributed with lower values than that at the center line, which might be caused by the slight overheating at this location and faster moisture removal rate. Below the center line, the relative values are also slightly lower than at the center. These results might have been caused by the relative location of sample and port as the heating is more concentrated at the top and edge parts. The microwaves distribution within the cavity also affected this phenomena.

As demonstrated in Figure 13, the microwaves distribution reflected by fax paper displayed a 2cm crest of the recorded waves, which could partly explained why the moisture content distribution at the upper parts was slightly different from the other portions of the sample.

5.2 Temperature

The temperature values of the sample were measured by the fiber optic sensor and transduced to Fiso-Commander software through a signal conditioner. The temperature readings were based on the average temperature recorded by the first 5 to 6mm from the sensor tip. Due to small radius (0.4mm) of the sensor tip, the tip's radius inserted into the sample was neglected. The temperature values obtained through simulation at different spatial locations were averaged along 5-6mm length of the sample basis using $T_{avg} = \frac{\int Tdl}{\int dl}$.

The temperature values at the core of the apple cylinder obtained from experiments and simulations were compared to validate the model.

Figures 17 demonstrates that the experimental temperature increases to 110 ℃ in about 17s and the predicted temperature increases gradually to 74 ℃. In general, the trend for the predicted temperature values agreed with that acquired from experiments indicated but the average absolute difference was 53.1%. Simulation results underestimated the temperature increase during the drying process. This might have been caused by the assumption that the sensor zone of the temperature probe was placed at 5mm to 6mm away from the bottom of the sample, while it varied slightly from this position. The evaporation of water throughout the sample due to heat absorption on the surface invoked the cooling phenomenon, which contributed to reduction in temperature values in the simulation (Rakesh and Datta, 2011). The temperature profiles obtained from the experiments tend to increase after a stable period. The mechanism for this temperature increase is not yet fully known. But, it could be caused by the phenomenon that the apple

tissue attached to the probe tip at high temperature during the drying process, which impeded the evaporation around the sensor tip and suppressed the cooling process. Also, the tissue attached to the tip might cause more heat transfer in the experiments, which led to the temperature increase. These analysis results proved that the model worked efficiently in predicting the temperature change tendency during the microwave drying process.

Initially, the temperature was assumed to be uniformly distributed within the sample (23.75℃), which was the same as the room condition. From the slice plots, it is evident that the temperature at the core is slightly lower than that on the surface at 30s, 60s and 120s drying (Figure 18a-c). This temperature distribution is in agreement with the moisture loss phenomenon, as higher temperature zone has higher evaporation rate and causes more moisture loss. The edge and corner effects also contributed to the higher edge temperature at the top parts. As microwaves can impinge into the sample from several directions at edges and corners, there is high intensity of electromagnetic fields at these locations of the sample, which causes the non-uniform temperature distribution. Due to the limited power absorption of the small sized sample, the sample could not absorb more power and attained more uniform temperature distribution after 180s of drying.

To understand if the temperature is distributed differently along the radius, the spatial distribution of temperature values with respect to the values at the center along the radius of the sample was plotted for three different locations: at the center line, 5mm above the center line and 5mm below the center line (Figure 19a-c). At these three locations, the relative temperature values on the surface were slightly higher than at the center. This

performance was consistent with the moisture content behavior as higher temperature portion caused more moisture loss. At 300s, the relative temperature (T/T_{center}) along the radius approached 1, which demonstrated the uniform temperature distribution toward the last stage of drying.

During the drying process, the temperature increases gradually and overheating was depressed due to the increased evaporation phenomenon, which is a cooling process. The evaporation rate is plotted at 30s, 60s and 120s drying in slices at x-y plane (Figure 20a-c). It is evident that the evaporation rate was low at 30s drying, which was 0.00171 kg/m^3s (Figure 20a). At 60s, the evaporation rate was higher at the surface and reached 0.00282 kg/m^3s (Figure 20b). At the initial drying stages, the evaporation mainly focused on the surface and edges of the sample. After 120s drying, the evaporation occurred throughout the whole sample and the evaporation depressed slightly at the top surface.

The spatial profiles for evaporation rate along the radial vector from the center toward the surface of cylinders were plotted at three different locations: 5mm above the center line, 5mm below the center line, and at the center line (Figure 21a-c). For the first minute, the evaporation term was in negative value, which was caused by the rapid moisture removal in the first minute. High evaporation rate on the surface developed higher vapor pressure and subsequently led to the liquid condensation. After that, the rate of evaporation increased and evaporation occurred mainly near the surface.

5.3 Mechanical properties

Apple tissues shrink during the drying process and the shrinkage extent is closely related to the mechanical properties of the porous material. Young's modulus of elasticity (E_w) was plotted during the microwave drying process (Figure 22a-c). As the drying proceeded, the E_w value increased and it was slightly higher at the top surface and edges compared to that of the center portions, which was caused by the fast moisture removal at these regions. This performance is also consistent with the moisture and temperature distribution as discussed in previous sections. During the drying process, as the moisture is removed from the sample, its E_w increases due to the higher solid portion.

5.4 Improvements of parameters

Based on the previous discussions, the moisture content values obtained from experiment and simulation are in a good agreement. However, for the temperature, the values obtained from simulation slightly underestimate the experimental temperature. So the related parameters were studied to see how they affect the heat transfer process in the porous media.

5.4.1 Heat conductivity

As the heat conductivity is closely related to the heat conduction phenomenon, the heat conductivity was varied according to the base value obtained from the previous study. The value of 0.4, 0.5 and 0.6 $W/m \cdot K$ were studied. The moisture content and temperature

distribution was plotted in Figure 23a-c and Figure 24a-c. From the plots, it is obvious that the variation of heat conductivity values alone did not significantly affect the drying process.

5.4.2 Moisture diffusion coefficient

The moisture diffusion coefficient affects its ability to diffuse during the drying process. In the microwave drying, the oscillation of water molecules increased and the moisture diffusivity values were accordingly increased ($1 \cdot Dw, 10 \cdot Dw, 100 \cdot Dw$) to study whether they would impact the drying process greatly. The moisture content profiles at three different diffusivity values are plotted in Figure 25. Even when the diffusivity value was increased greatly, the moisture content profiles were in consistent with each other and this variation study did not demonstrate that the diffusivity would affect moisture content performance.

Based on these trial studies, the discrepancy between predicted and experimental temperature values could not be reduced by the variation of single factor. For the next step, combination of parameters and more experiments are recommended to determine the reasons that caused this discrepancy.

6. Summary and Conclusions

In this study, the fluid transport mechanisms and the microwave operation principles during microwave drying were elucidated. The mathematical model was built based on the generalized fluid transport equations, heat balance and electromagnetic wave equations. In order to validate the model, the microwave drying experiments with apple cylinders were conducted at 550W. The comparison of moisture content profiles obtained from experiments and simulations demonstrated a good fit, which validated the efficiency of the built model for fluid transport. This showed that the hybrid mixture theory based fluid transport model coupled with the electromagnetic wave equation were capable of predicting the transport mechanisms for the microwave drying of apple cylinders. Based on the analysis of results, this model could be applied in predicting the moisture loss within the sample under microwave drying conditions. For the temperature distribution, the variation of related parameters was conducted, which did not produce a good solution to decrease the discrepancy between predicted and experimental values. Further work is recommended on reducing this discrepancy based on performing a broader parametric sweep and conducting additional experiments.

Nomenclature

Latin symbols

a_w	Water activity of the porous matrix
$\boldsymbol{B}$	Magnetic flux density (Tesla)
C_p^α	Specific heat of phase α (J/kg°K)
D^α	Coefficient of diffusivity of the phase α (m^2/s)
${}^\beta\hat{e}^\alpha$	Net rate of mass transfer from the phase β to the phase α (kg/m^3 s)
$\boldsymbol{E}$	Electric field intensity (V/m)
$\boldsymbol{E}_s$	Source electric field strength (V/m)
E_M	Young's modulus (Pa)
ϕ	Porosity of sample $\phi = \varepsilon^w + \varepsilon^g$
G^α	Gibbs free energy of the phase α (J/kg)
$\boldsymbol{H}$	Magnetic field intensity (A/m)
h_{mw}	Mass transfer coefficient for water phase (m/s)
h_{mv}	Mass transfer coefficient for vapor phase (m/s)
h_T	Heat Transfer coefficient ($W/(m^2°K)$

$\boldsymbol{J}$	Electric current density (A/m^2)
k^{α}	Thermal conductivity of the α phase (W/(m°K))
k_0	Wave number
K^{α}	Permeability of the α phase (m^2)
L	Characteristic length of the sample (m)
M	Moisture content on dry basis (g/g solids)
N^{α}	Mixture viscosity (Pa·s)
p^{α}	Physical pressure in the phase α (Pa)
p_{veq}	Pressure of water in the vapor phase at equilibrium state (Pa)
p_{atm}	Atmospheric pressure (Pa)
p_c	Capillary pressure (Pa)
Q_w	Surface water flux (m/s)
Q_v	Surface vapor flux (m/s)
Q_m	Microwave heat source (W/m^3)
R	Specific gas constant for water vapors (J/ (kg·K))
S_w	Water saturation (dimensionless)

σ Electrical conductivity (S/m)

σ_s Stefan-Boltzman constant (5.670373×10^{-8}W/ (m^2°K^4))

T Temperature (°K)

T_{amb} Ambient temperature (°K)

t Time (s)

v_{total} Volume of the whole sample (m^2)

$\boldsymbol{v}_l^{\alpha}$ Velocity of the α phase (m/s)

$\boldsymbol{v}^{\alpha,s}$ Velocity of the α phase relative to the solid phase (m/s)

$\boldsymbol{v}^{v,g}$ Velocity of vapor phase relative to the gas phase (m/s)

V_{water} Volume of pure water (cm^3)

ξ^v Near equilibrium evaporation rate coefficient

Greek symbols

ε^{α} Volume fraction of the α phase (dimensionless) $\varepsilon^{\alpha} = \frac{\mathrm{v}_{\alpha}}{\mathrm{v}_{total}}$

ε Coefficient of emissivity (dimensionless)

$\varepsilon^{'}$ Dielectric constant

$\varepsilon^{''}$ Dielectric loss factor

ε_r Relative permittivity (dimensionless)

ε_0 Permittivity for free space (F/m)

λ Latent heat of vaporization (J/kg)

μ^α Viscosity of the α phase in the porous matrix (Pa·s)

μ_r Relative permeability (dimensionless)

ω Angular frequency (rad/s)

ρ^α Density of the phase α (kg/m^3)

Subscripts

i Initial

l Indices for Eulerian coordinates

Superscripts

α General representation of a phase

β General representation of a phase

s Solid phase

w Water phase

g Gas phase

v	Vapor phase
pre	Predicted
exp	Experimental

References

Achanta, S., Cushman, J. H., 1994. Nonequilirbium swelling-pressure and capillary-pressure relations for colloidal systems. J. Colloid Interface Sci. 168 (1), 266-268.

Achanta, S., Okos, M. R., Cushman, J. H., Kessler, D. P., 1997. Moisture transport in shrinking gels during saturated drying. *AIChE Journal*, 43(8):2112-2122.

Andres, A., Bilbao, C., Fito, P., 2004. Drying kinetics of apple cylinders under combined hot air-microwave dehydration. Journal of Food Engineering 63(1):71-78.

AOAC,1990. Official Methods of Analysis. 15th ed. Washington, D.C.: Association of Official Analytical Chemists.

Bennethum, L. S., Cushman, J. H., 1999. Coupled solvent and heat transport of a mixture of swelling porous particles and fluids: single time-scale problem. *Transport in Porous Media* 36:211-244.

Bird, R. B., Stewart, W. E., Lightfoot, E. N., 2006. *Transport Phenomena*, 2nd edition. Hoboken, NJ: John Wiley & Sons, Inc.

Chen, G., Wang, W., Mujumdar, A. S., 2001. Theoretical study of microwave heating patterns on batch fluidized bed drying of porous material. *Chemical Engineering Science* 56, 6823-6835.

Coleman, B. D., Noll, W., 1963. The thermodynamics of elastic materials with heat conduction and viscosity. *Archive for Rational Mechanics and Analysis* 13, 167-178.

COMSOL Release history. (2013, November 27). . Retrieved June 10, 2014, from http://www.comsol.com/support/releasehistory/

de Vries, D. A., 1958. Simultaneous transfer of heat and moisture in porous media. *American Geophysical Union* 39(5), 909-916.

Dibben, D., 2001. Electromagnetics: Fundamental Aspect and Numerical Modeling. *Handbook of Microwave Technology for Food Applications*. New York, NY: Marcel Dekker, Inc.

Duan, X., Ren, G. Y., Zhu, W. X., 2012. Microwave Freeze Drying of Apple slices based on the dielectric properties. *Drying Technology* 30, 535-541.

Fang, G., Ward, C. A., 1999. Examination of the statistical rate theory expression for liquid evaporation rates. Phys. Rev, e 59 (1), 441-453.

Feng, H., Tang, J., Dixon-Warren, S. J., 2000. Determination of moisture diffusivity of red delicious apple tissues by thermo gravimetric analysis. *Drying Technology* 18, 1183-1199.

Feng, H., Tang, J., Cavalieri, R. P., 2002. Dielectric properties of dehydrated apples as affected by moisture and temperature. *American Society of Agricultural Engineers* 45(1): 129-135.

Feng, H., Tang, J., Cavalieri, R. P., Plumb, O. A., 2001. Heat and Mass transport in microwave drying of porous materials in a spouted bed. *AIChE Journal* 47 (4), 1499-1512.

Feng, H., Tang, J., Plumb, O. A., Cavalieri, R. P., 2004. Intrinsic and relative permeability for flow of humid air in unsaturated apple tissues. *Journal of Food Engineering* 62:185-192.

Fuller, A. J. B. 1990. Microwaves: an introduction to microwave theory and techniques. Pergamon Press, Oxford, UK.

"Full Report (All Nutrients): 09003, Apples, Raw, with Skin." *USDA National Nutrient*. N.p., n.d. Web. 25 May 2014. <http://ndb.nal.usda.gov/ndb/foods/show/2200?qlookup=09003&format=Full&max=25&man=&lfacet=&new=1>.

"Food and Agricultural Commodities Production." *Food and Agriculture Organization of the United States*. N.p., n.d. Web. 25 Apr.2014. <http://faostat.fao.org/site/339/default.aspx>.

Geedipalli, S. S. R., Rakesh, V., Datta, A. K., 2007. Modeling the heating uniformity contributed by a rotating turntable in microwave ovens. *Journal of Food Engineering* 82(3), 359-368.

Hellebrand, H. J., Beuche, H., Linke, M., 2001. Determination of thermal emissivity and surface temperature distribution of horticultural products. In: Sixth International Symposium on Fruit, Nut and Vegetable Production Engineering, Potsdam, Germanly.

"The IEEE standard dictionary of electrical and electronics terms", 6th ed. New York, N. Y., Institute of Electrical and Electronics Engineers, c1997. IEEE Std 100-1996. ISBN 1-55937-833-6.Khraisheh, M. A. M., Cooper, T. J. R., Magee, T. R. A., 1997. Microwave and air

drying I. Fundamental considerations and assumptions for the simplified thermal calculations of volumetric power absorption. *Journal of Food Engineering*, 33, 207-219.

Krokida, M. K., Maroulis, Z. B., 1999. Effect of microwave drying on some quality properties of dehydrated products. *Drying Technology*, 17, 449.

Leverett, M. C., 1941. Capillary behavior in porous solids. *AIME Transactions*, 142, 152-169.

Mudget, R. E., 1986. Electrical properties of foods, Ch. 7. *In Engineering Properties of Foods*, eds. M. A. Rao, and S. S. H. Rizvi. New York, N. Y.:Marcel Dekker, Inc.

Metaxas, A.C., Meredith, R. J., 1983. Industrial microwave heating. *Institute of Electrical and Electronics Engineers*. London, U.K.: Peter Peregrinus Ltd.

Mujumdar, A. S., 2004. Research and development in drying: recent trends and future prospects. *Drying Technology* 22(1-2), 1-26.

Ni, H., Datta, A. K., K., Torrance, K. E., 1999. Moisture transport in intensive microwave heating of biomaterials: a multiphase porous media model. *International Journal of Heat and Mass Transfer* 42, 1501-1512.

Nellis, G., Klein, S., 2008. Heat Transfer, 1 st edition Cambridge University Press, Cambridge, UK.

Pakowski, Z., Adamski, R., 2012. Formation of under pressure in an apple cylinder during convective drying. *Drying Technology* 30, 1238-1246.

Pere, C., Rodier, E., 2002. Microwave vacuum drying of porous media: experimental study and qualitative considerations of internal transfers. *Chemical Engineering and Processing* 41, 427-436.

Perry, R. H., Green, D. W., 2008. Perry's Chemical Engineering Handbook. McGraw Hill, New York, USA.

Rakesh, V., Datta, A. K., 2011. Microwave puffing: Determination of optimal conditions using a coupled multiphase porous media-Large deformation model. *Journal of Food Engineering* 107, 152-163.

Rahman, M. S., Chen, X. D., Perera, C. O., 1997. An improved thermal conductivity prediction model for fruits and vegetables as a function of temperature, water content and porosity. *Journal of Food Engineering* 21(2), 163-1

Ratti, C., Crapiste, G. H., 1995. Determination of heat transfer coefficients during drying of foodstuffs. *Journal of Food Process Engineering*, 18, 41-53.

Ryynanen, S. 1995. The electromagnetic properties of food materials: A review of the basic principles. *J. Food Eng*. 29(4):409-429.

Singh, P. P., Cushman, J. H., Maier, D. E., 2003. Multiscale fluid transport theory for swelling biopolymers. *Chemical Engineering Science* 58, 2409-2419.

Schiffmann, R. F., 2006. Microwave and Dielectric Drying. In Mujumdar, A. S. (3rd Ed.), *Handbook of Industrial Drying* (pp.286-305). Boca Raton, FL: CRC Press.

Schoeber, W. J. A. H., 1976. Regular Regimes in Sorption Processes. Ph.D. Thesis, Eindhoven University of Technology, the Netherlands.

Spencer, P. L., 1950. Method of treating foodstuffs, *US patent* 2495429.

Takhar, P. S., 2011a. Hybrid mixture theory based moisture transport and stress development in corn kernels during drying: coupled fluid transport and stress equations. *Journal of Food Engineering* 105, 663-670.

Takhar, P. S., Maier, D. E., Campanella, O. H., Chen, G., 2001b. Hybrid mixture theory based moisture transport and stress development in corn kernels during drying: Vlidation and simulation results. *Journal of Food Engineering* 206, 275-282.

Takhar, P. S., 2014. Unsaturated fluid transport in swelling poroviscoelastic biopolymers. *Chemical Engineering Science* 109, 98-110.

Tang, J., 2005. Dielectric properties of food. In The Microwave Processing of Foods; Schubert, H., Reglier, M., Eds.; Woodhead Publishing Ltd.: Cambridge, UK; 22–40.

Vollmer, M., 2004. Physics of microwave oven. *Physics Education* 39, 74-81.

Weinstein, T. F., 2005. Three-phase hybrid mixture theory for swelling drug delivery systems. (Unpublished doctoral dissertation). University of Colorado at Denver, Denver.

Zhang, H., Datta, A. K., 2005. Heating concentrations of microwaves in spherical and cylindrical foods Part one: in Plane Waves. *Food and Bioproducts Processing* 83, 6-13.

Appendix

Figures and Tables:

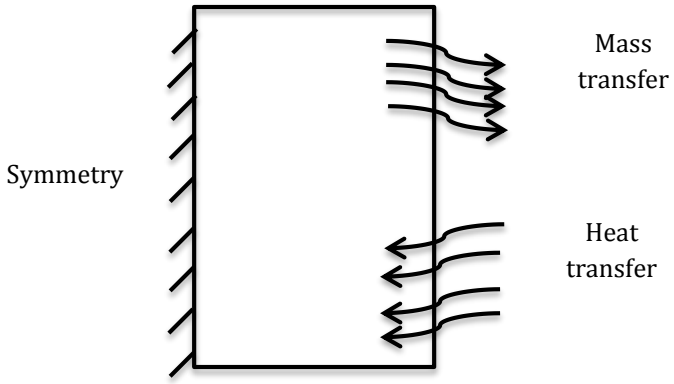

Figure 1. Diagram of the mass and heat transfer direction

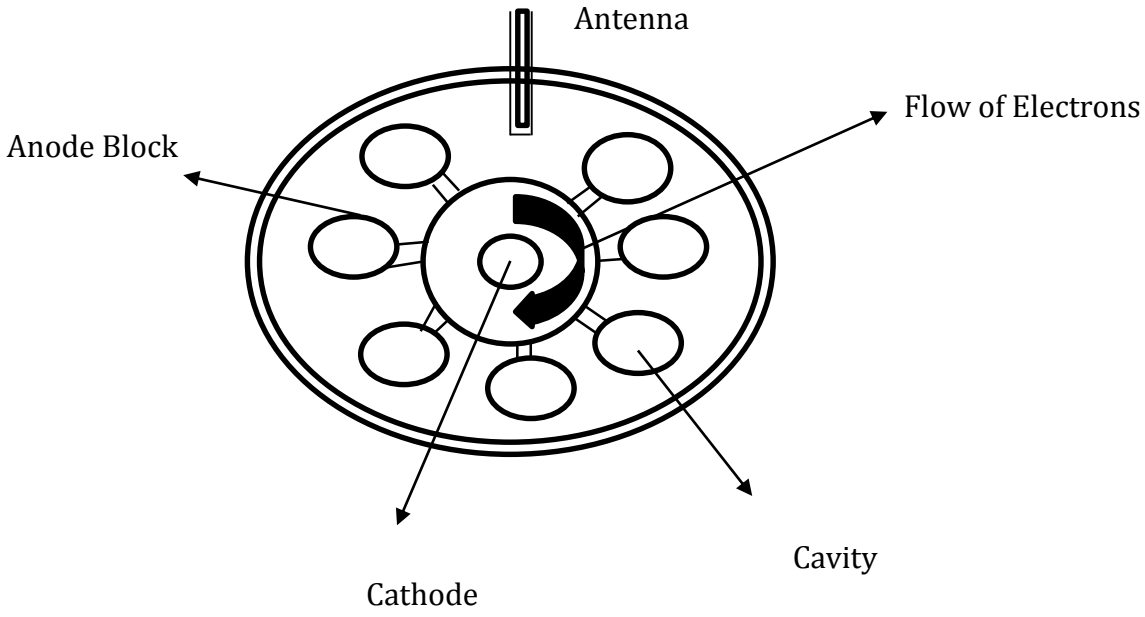

Figure 2. Magnétron structure

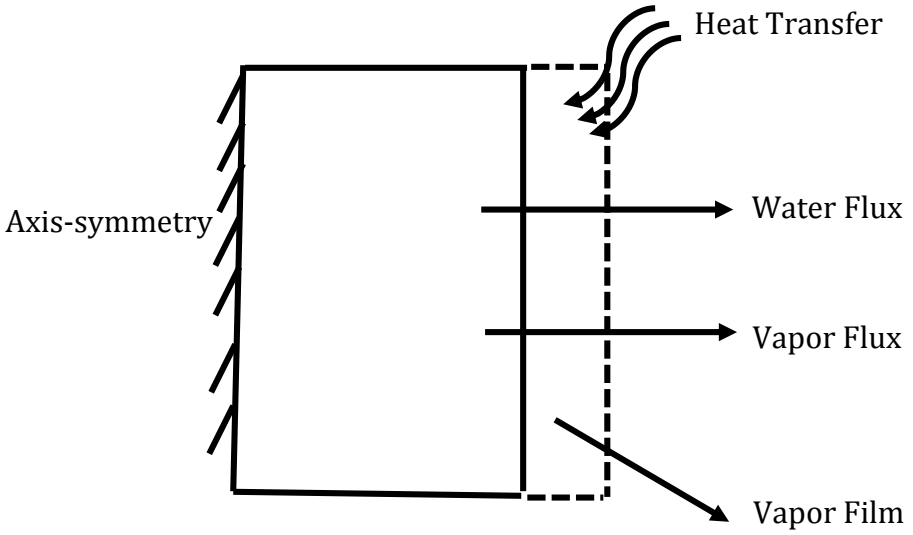

Figure 3. Schematic diagram of the mass and energy exchange at the boundary

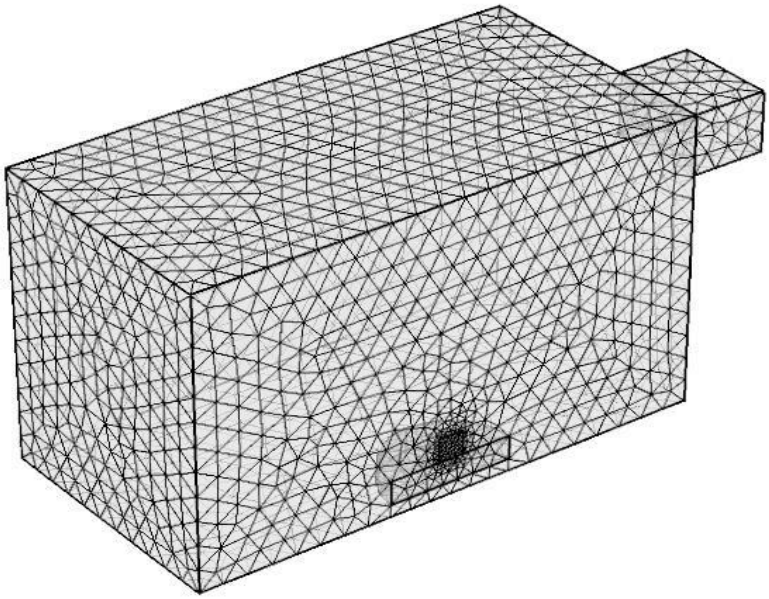

Figure 4. Finite element mesh for electromagnetic simulation in COMSOL Multiphysics (ver 4.4)

Figure 5. Panasonic NN-CD989S microwave/convection oven

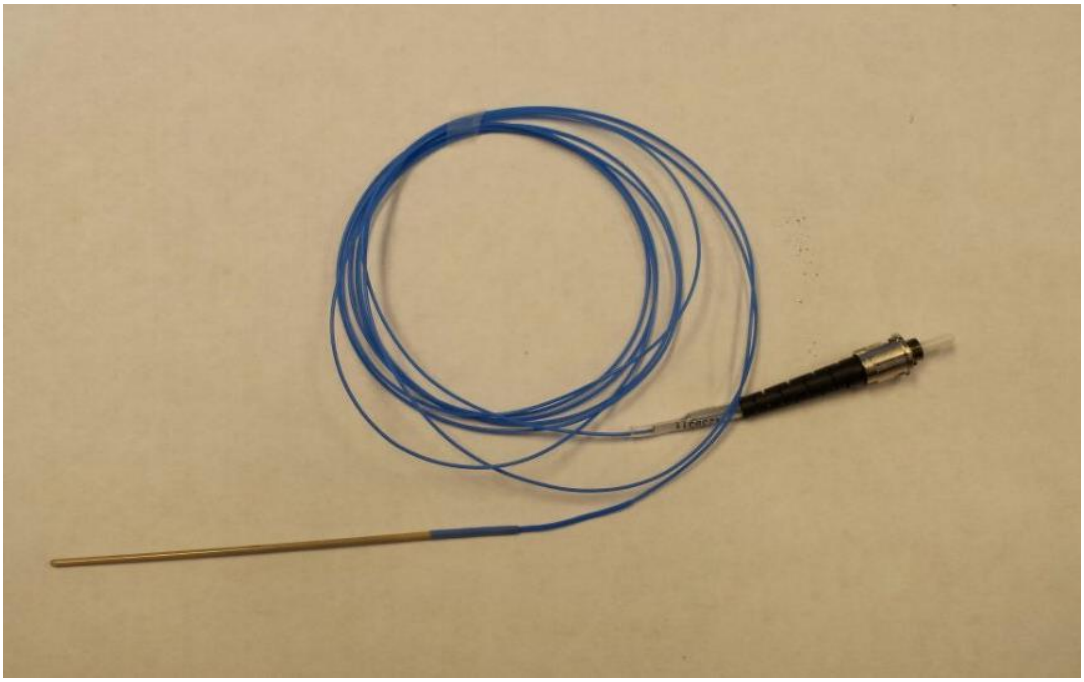

Figure 6. FOT-L-NS-825B fiber optic sensor (Fiso Technologies, 2013)

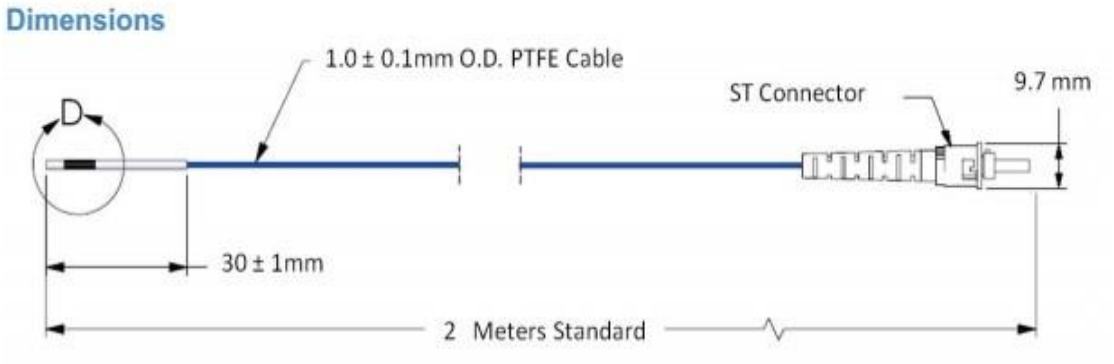

Figure 7. FOT-L-NS-852B dimensions (Fiso Technologies, 2013)

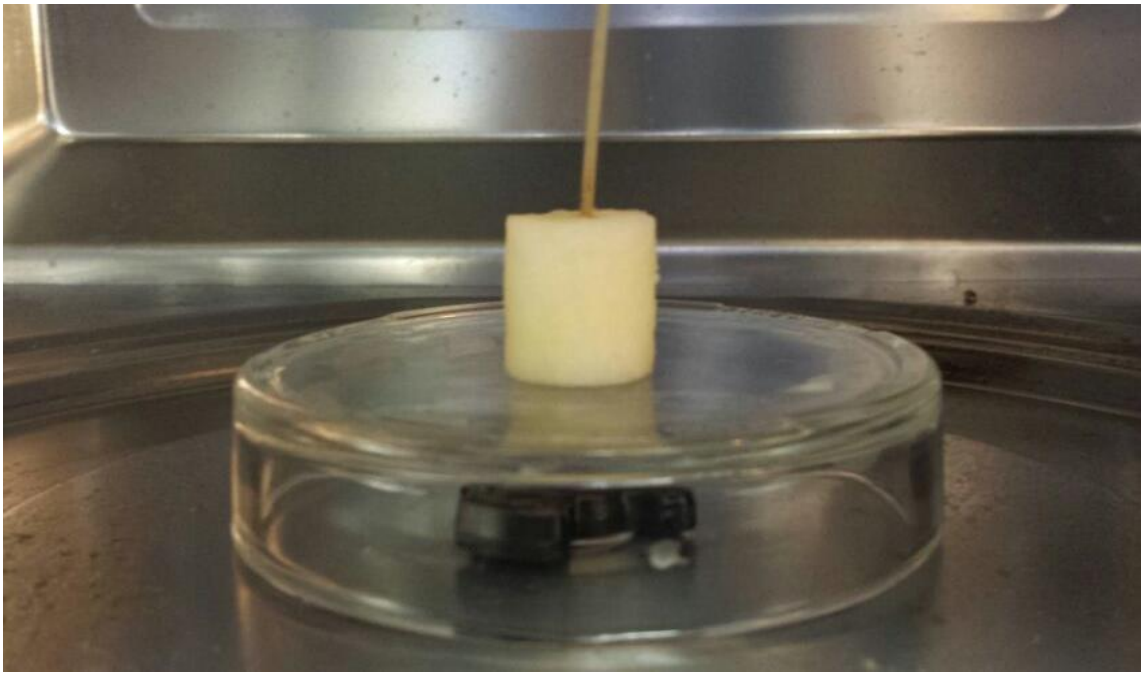

Figure 8. Location of sample and plate inside the microwave oven

Figure 9. OHAUS MB35 moisture analyzer (OHAUS Corporation)

Figure 10. FTI-10 Single-channel signal conditioner (Fiso Technologies, 2013)

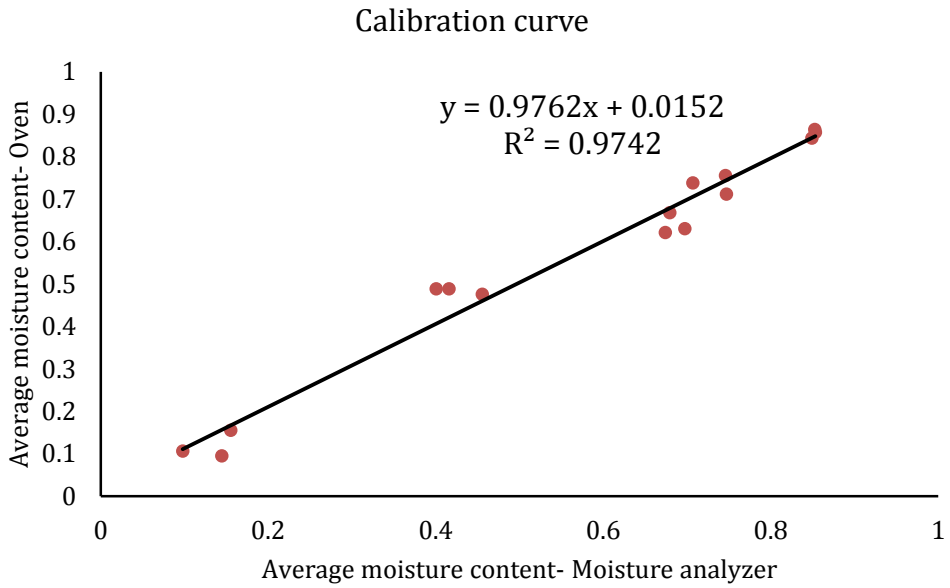

Figure 11. Calibration curve for moisture calculation between oven method and moisture analyzer method

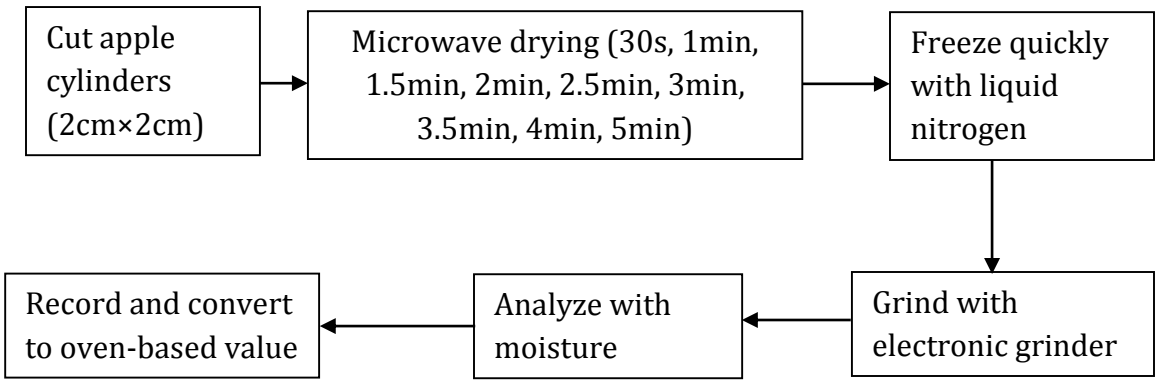

Figure 12. Flow chart of the experimental process

(a) (b)

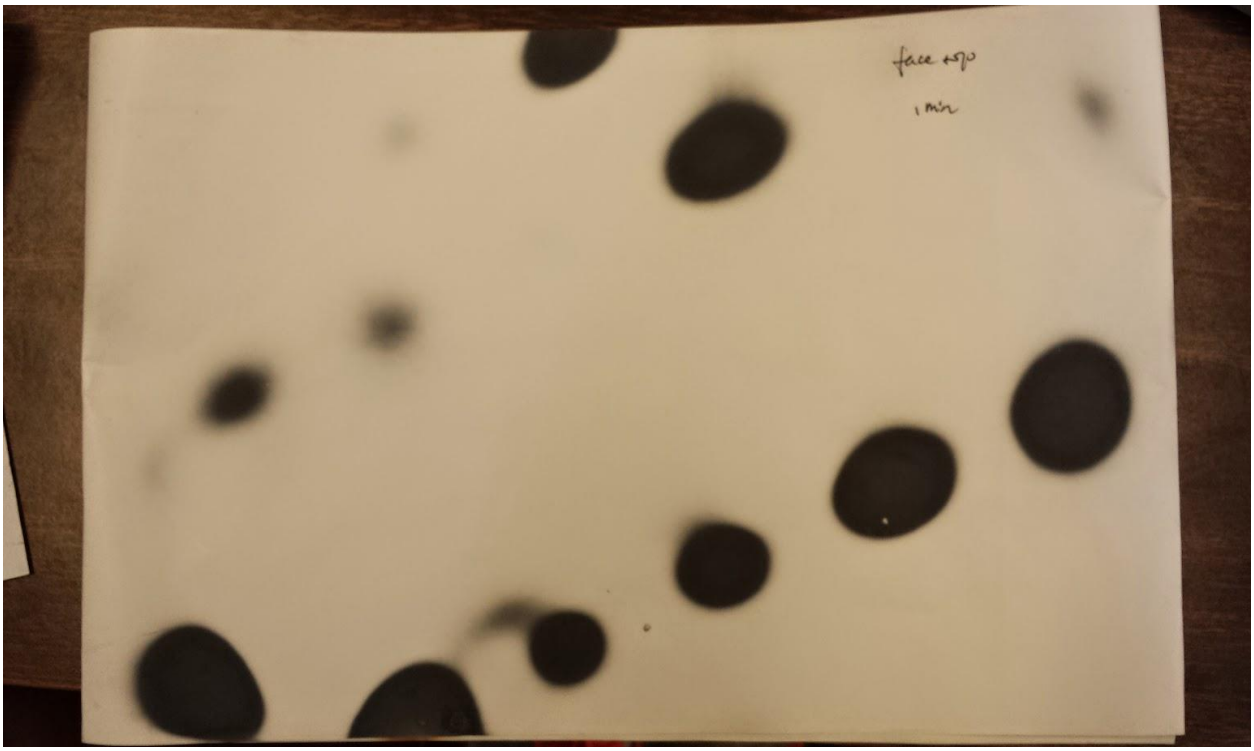

(c)

Figure 13(a)-(c). Microwaves condition and heating concentration reflected by fax paper after 1min heating

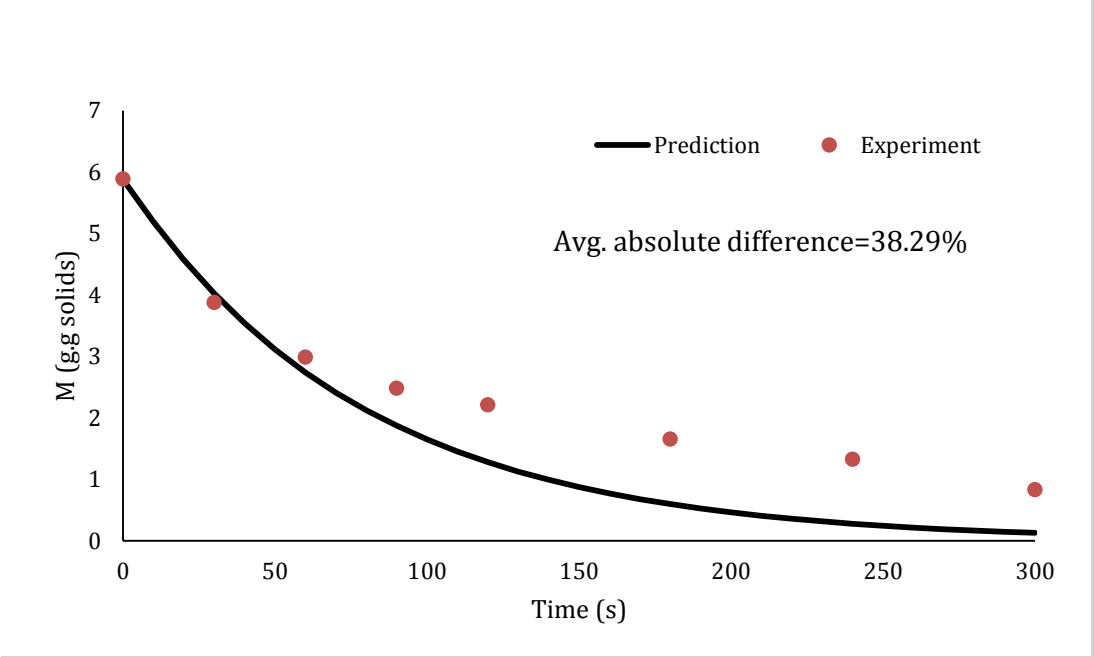

Figure 14. Averaged moisture content (g/g solids) within the sample at 550W

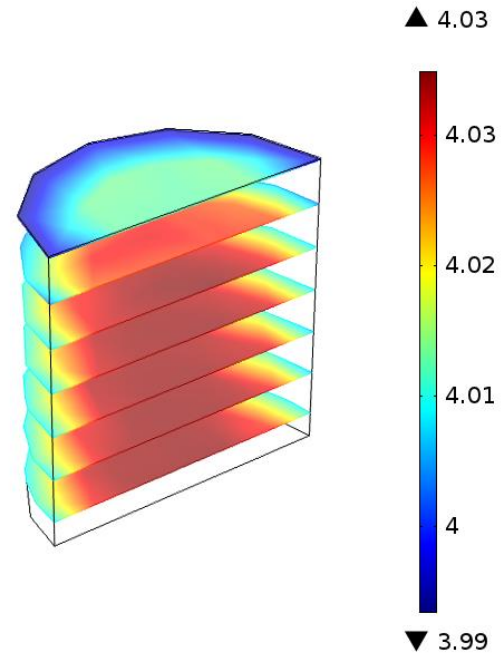

Figure 15a. Slice plots of moisture content (g/g solids) after 30s drying

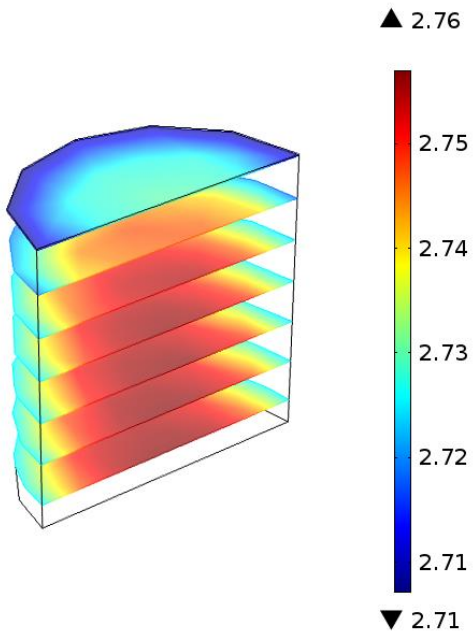

Figure 15b. Slice plots of moisture content (g/g solids) after 60s drying

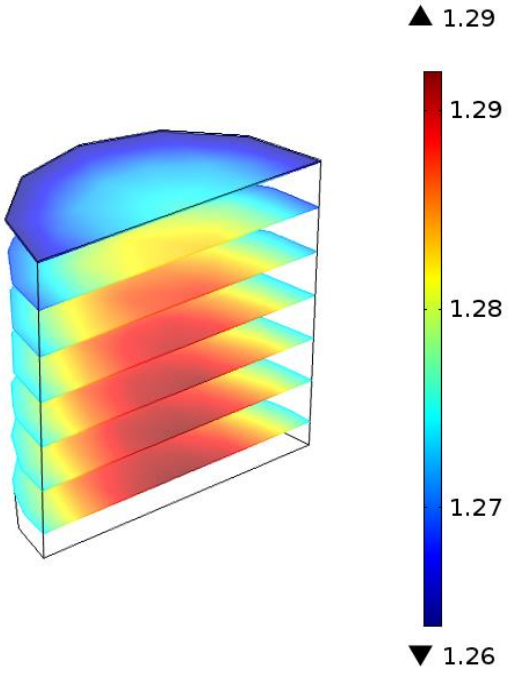

Figure 15c. Slice plots of moisture content (g/g solids) after 120s drying

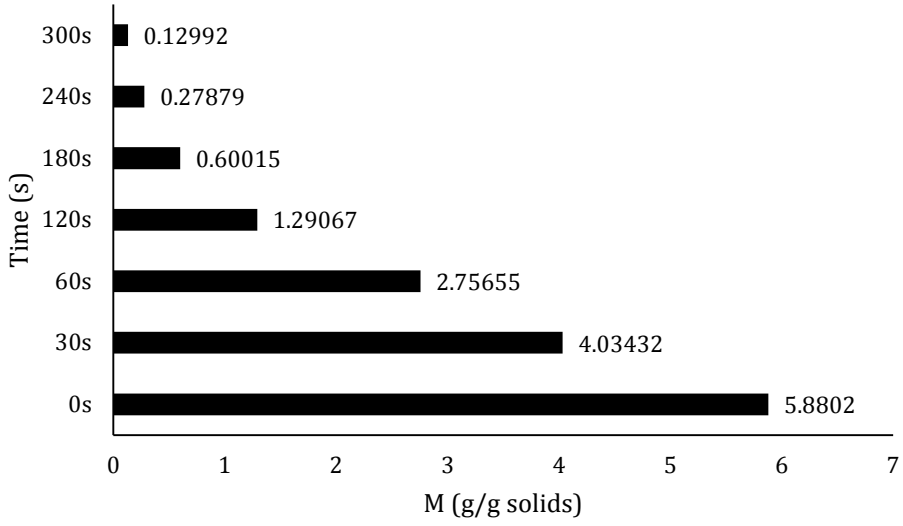

(1)

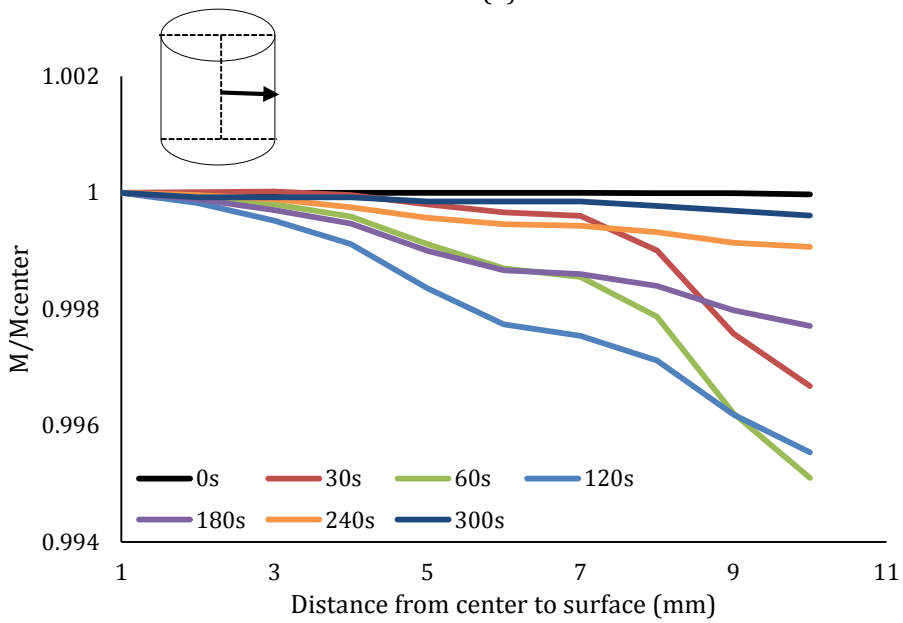

(2)

Figure 16a (1)-(2). Moisture content value at the center point at different drying time; spatial distribution of relative moisture content (with respect to the center point value) at the radial vector from center to surface of the cylinder (at center line)

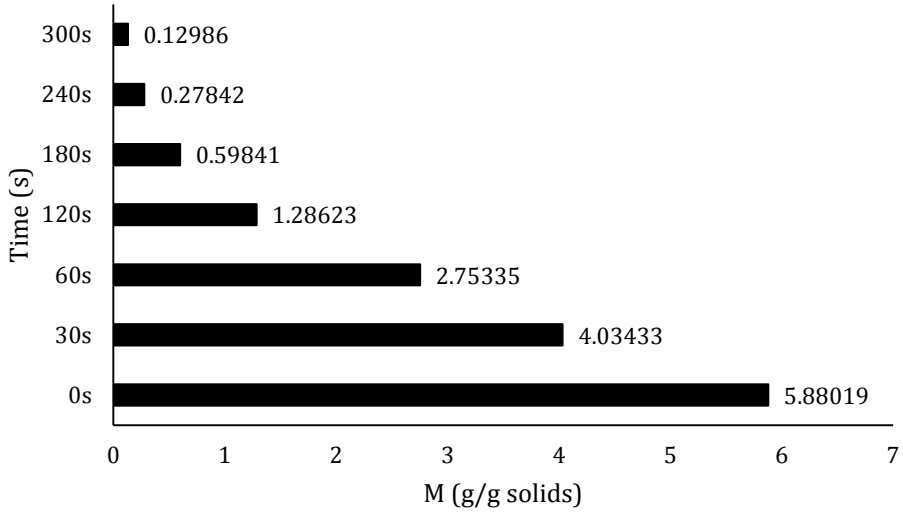

(1)

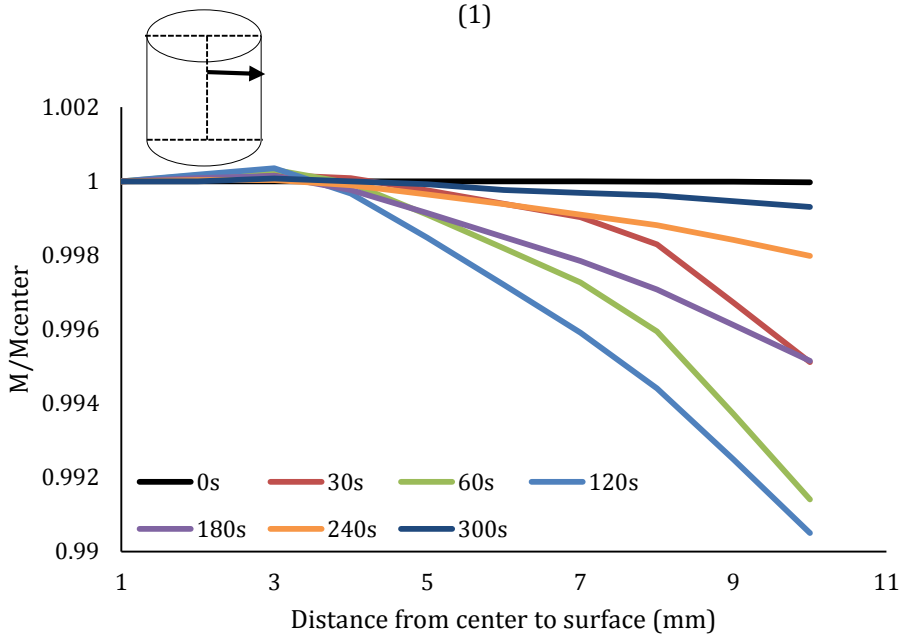

(2)

Figure 16b (1)-(2). Moisture content value at the center point at different drying time; spatial distribution of relative moisture content (with respect to the center point value) at the radial vector from center to surface of the cylinder (above the center line)

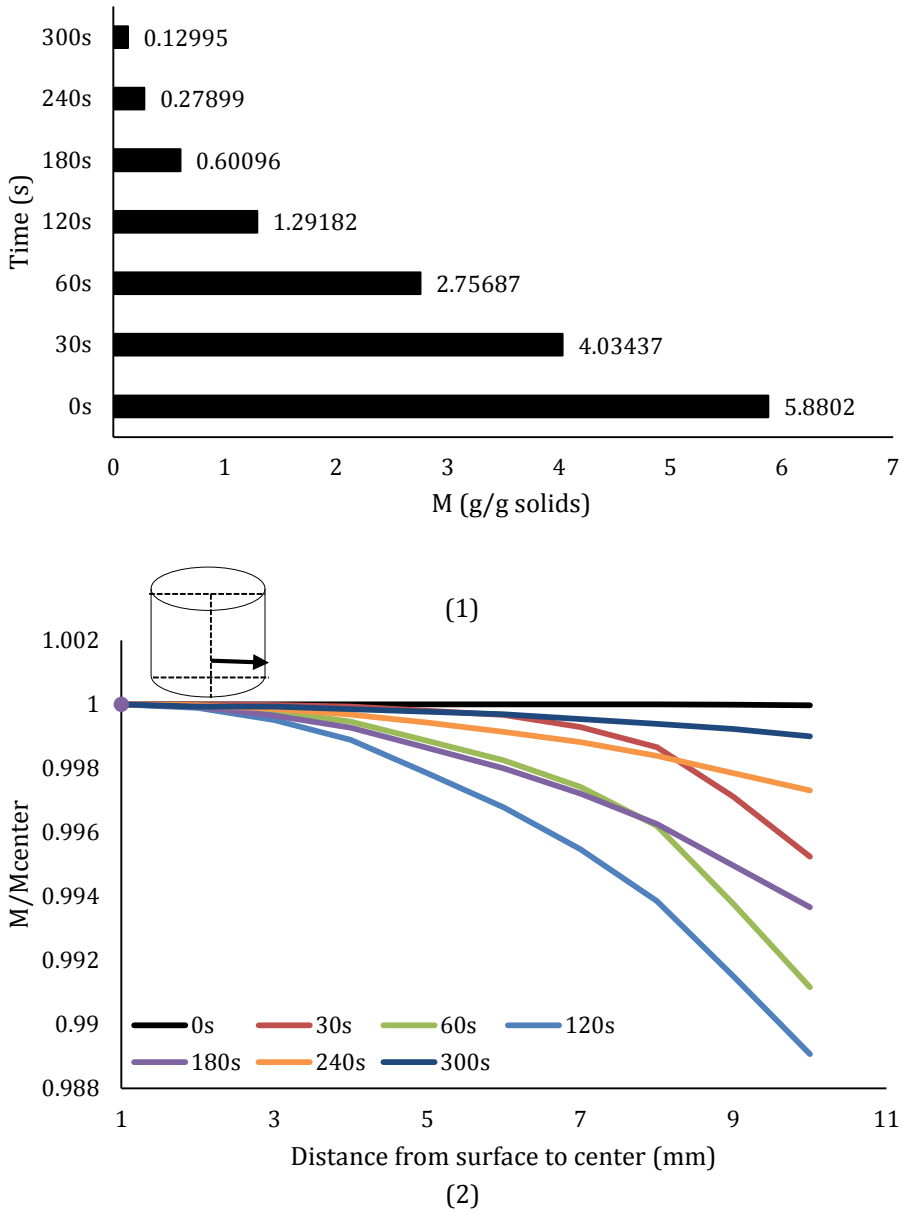

Figure 16c (1)-(2). Moisture content value at the center point at different drying time; spatial distribution of relative moisture content (with respect to the center point value) at the radial vector from center to surface of the cylinder (below the center line)

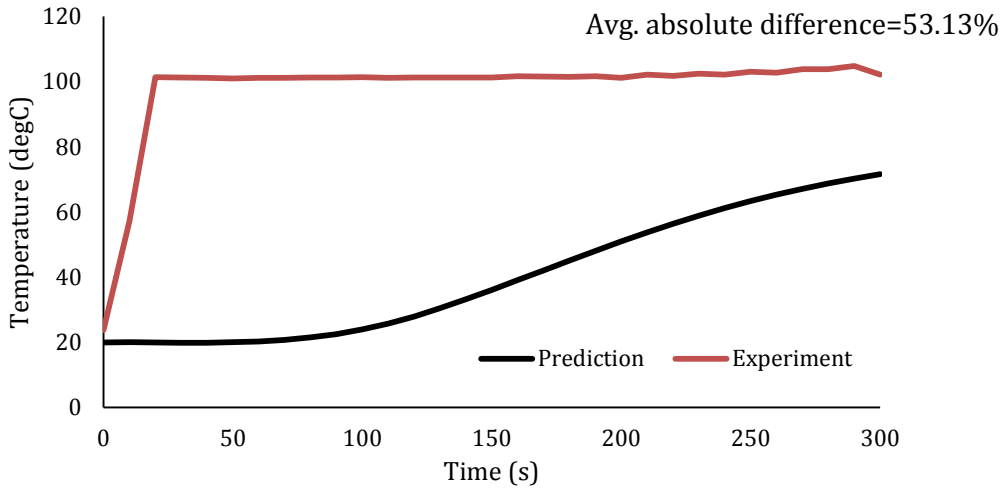

Figure 17. Line-averaged temperature (°C) within the smaple at 550W

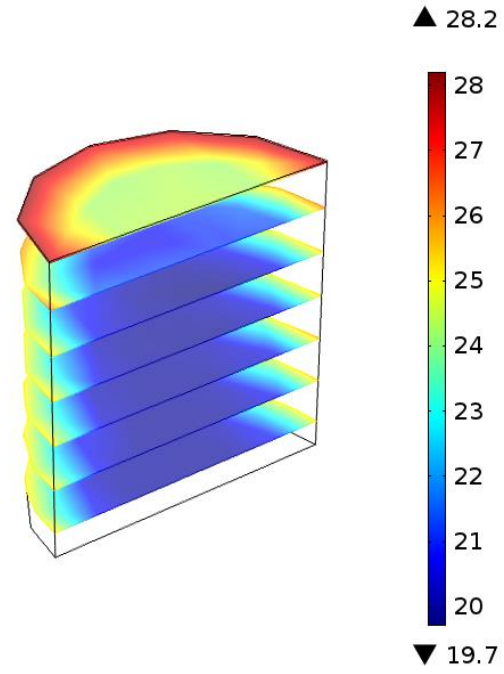

Figure 18a. Slice plots of temperature (°C) within the sample after 30s drying

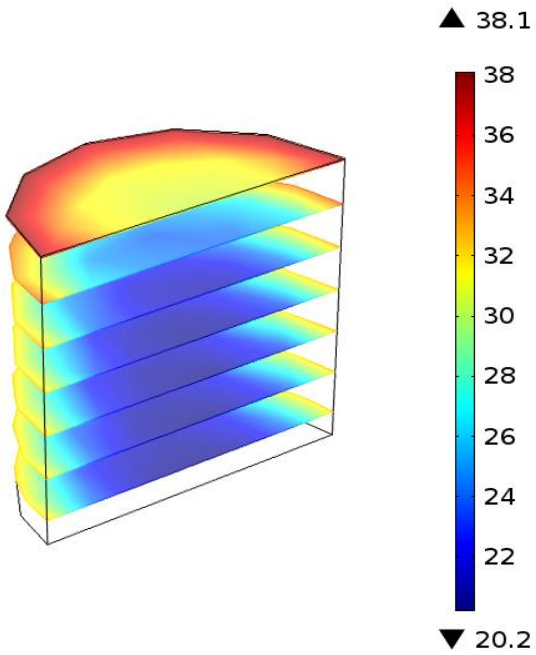

Figure 18b. Slice plots of temperature (°C) within the sample after 60s drying

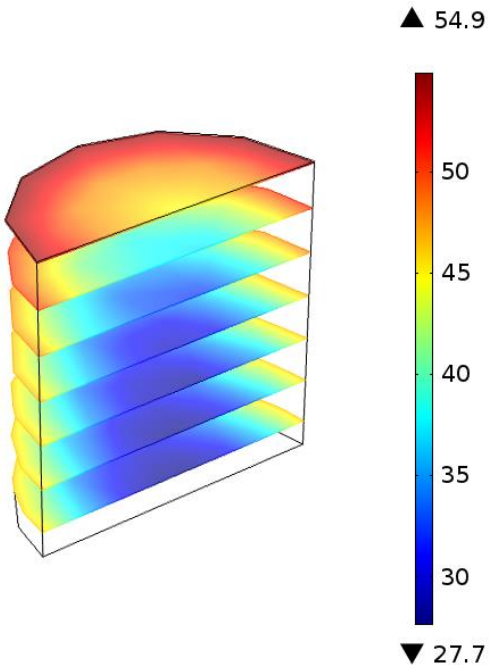

Figure 18c. Slice plots of temperature (°C) within the sample after 120s drying

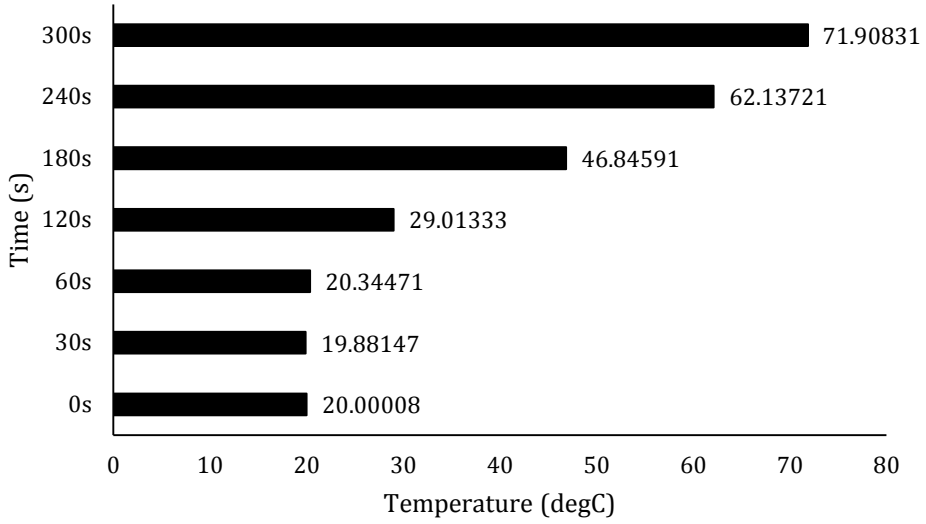

(1)

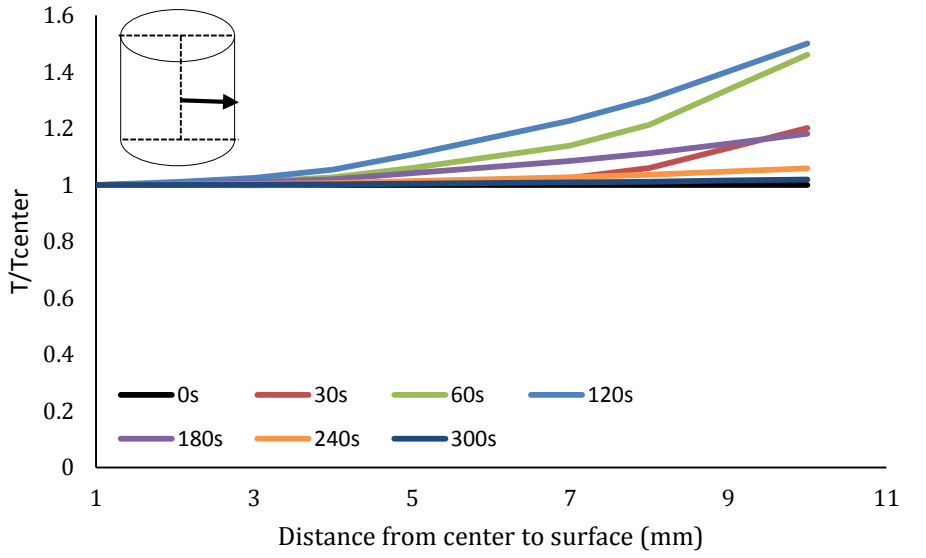

(2)

Figure 19a (1)-(2) Temperature value at center point at different drying time; spatial distribution of relative temperature values (with respect to the center point value) at the radial vector from center to surface of the cylinder (at center line)

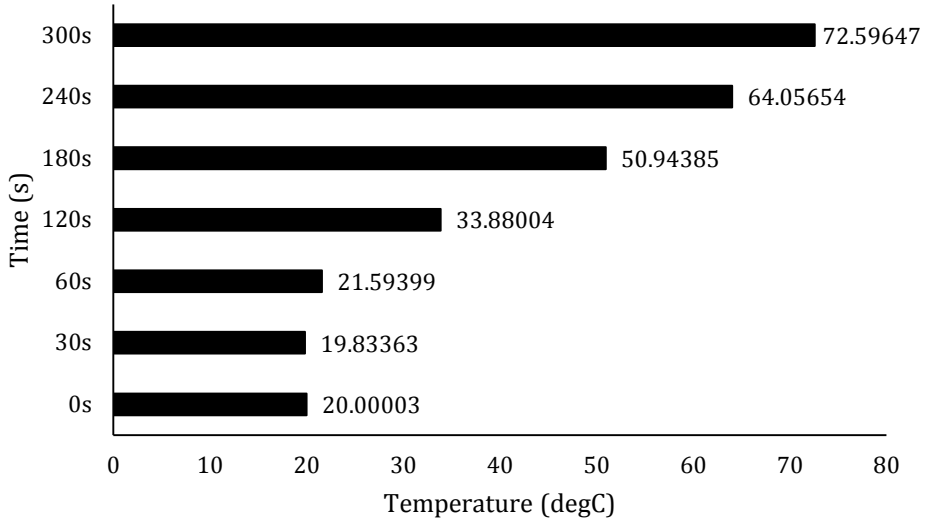

(1)

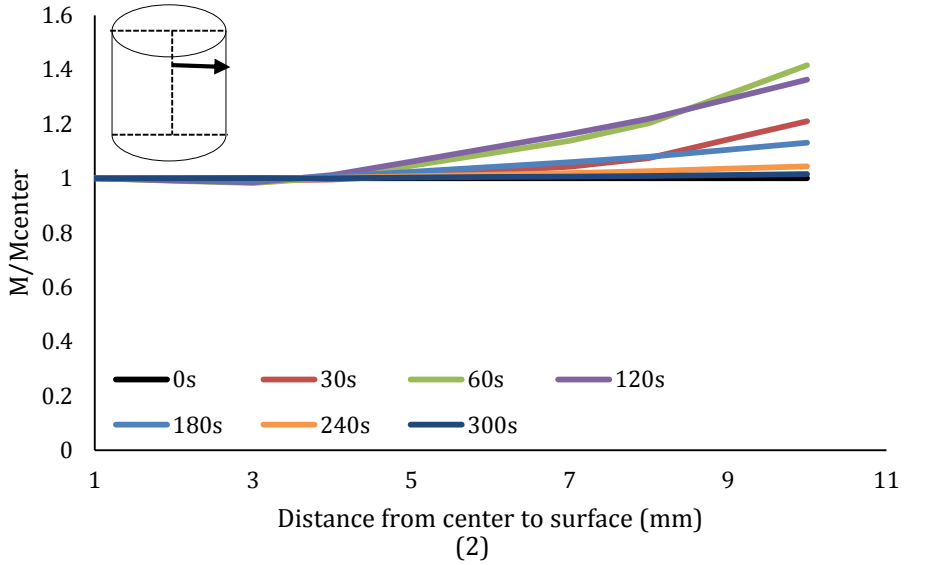

(2)

Figure 19b (1)-(2). Temperature value at the center point at different drying time; spatial distribution of relative temperature values (with respect to the center point value) at the radial vector from center to surface of the cylinder (above center line)

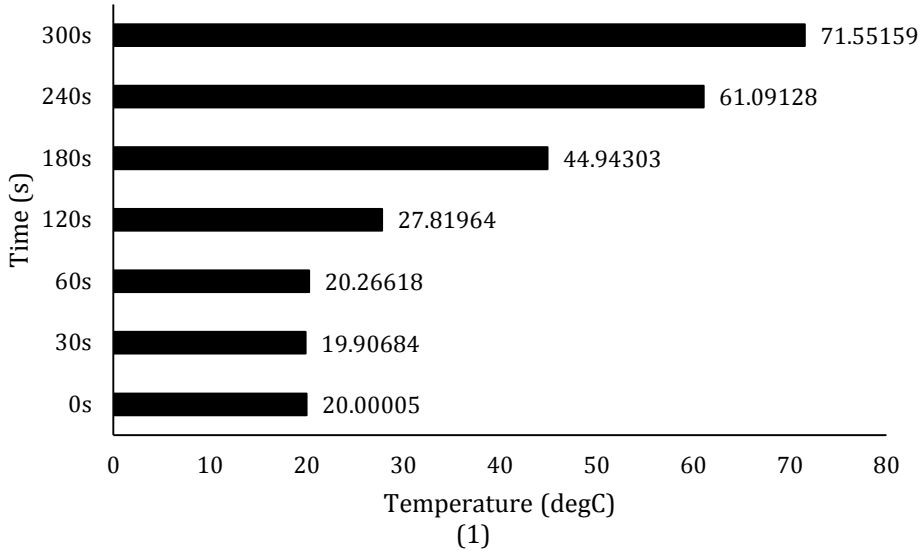

(1)

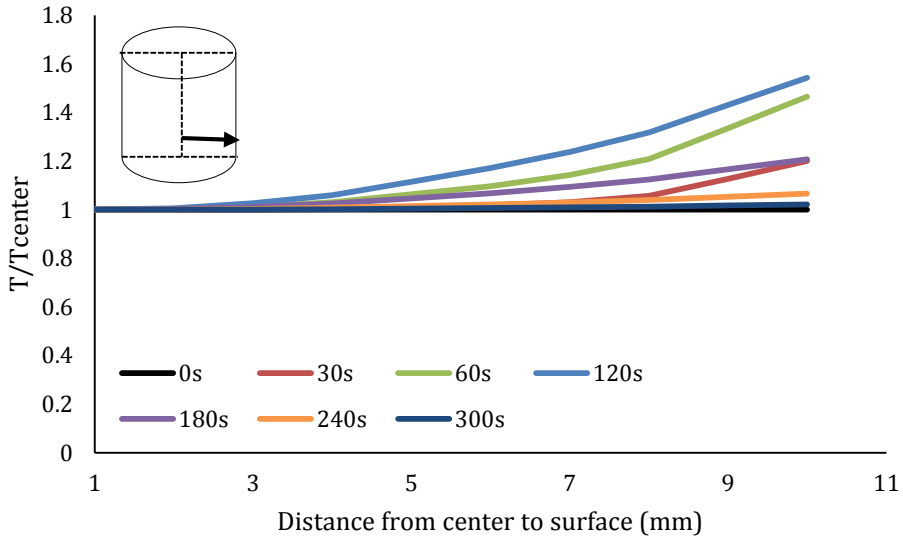

(2)

Figure 19c (1)-(2). Temperature value at center point at different drying time; spatial distribution of relative temperature values (with respect to the center point value) at the radial vector from center to surface of the cylinder (below center line)

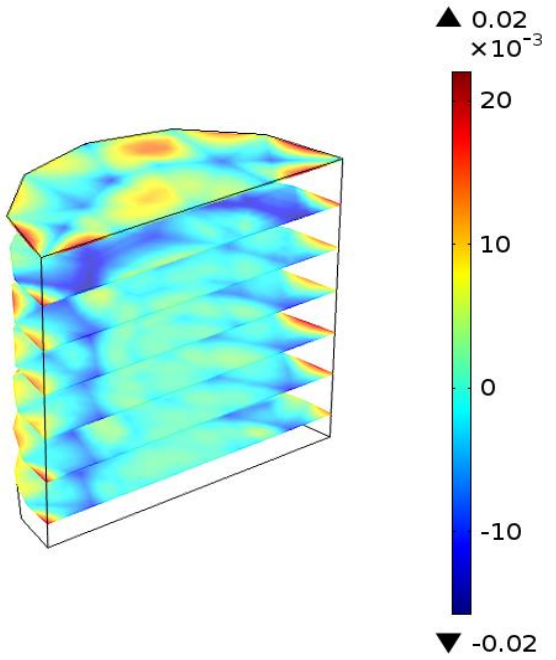

Figure 20a. Slice plots of evaporation rate (kg/m^3 s) within the sample after 30s drying

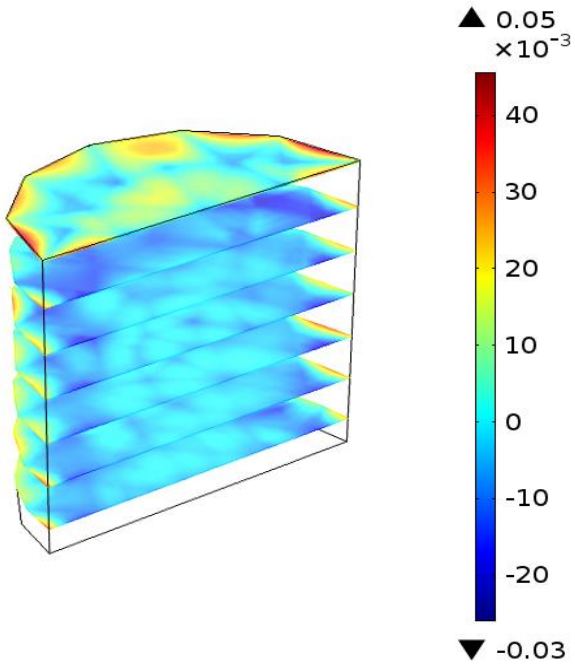

Figure 20b. Slice plots of evaporation rate (kg/m^3 s) within the sample after 60s drying

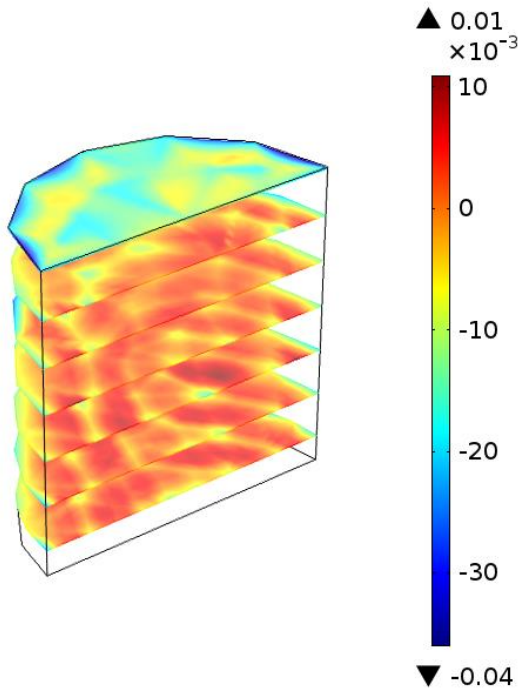

Figure 20c. Slice plots of evaporation rate (kg/m^3 s) within the sample after 120s drying

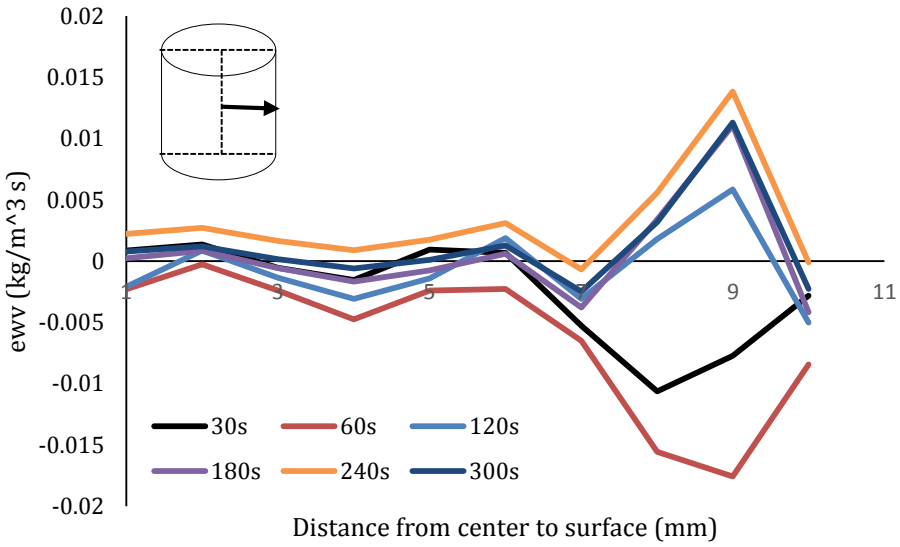

Figure 21a. Spatial distribution of evaporation rate (kg/m^3 s) within apple cylinders (at the center line)

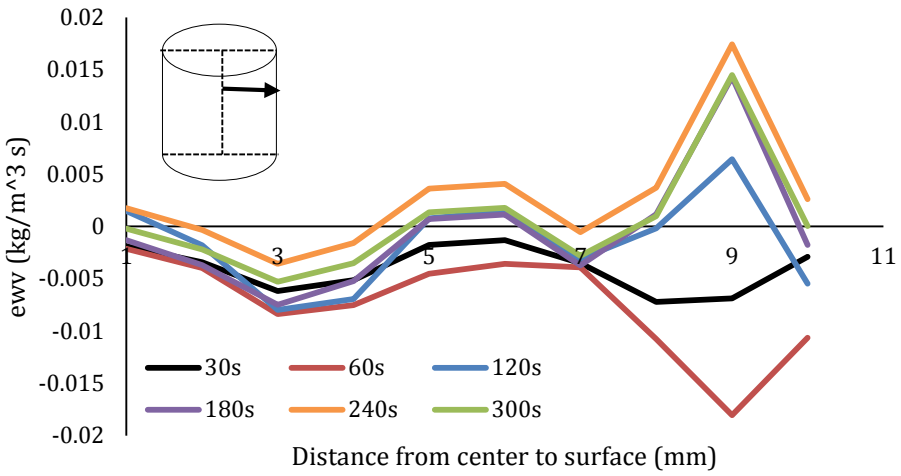

Figure 21b. Spatial distribution of evaporation rate (kg/m^3 s) within apple cylinders (above the center line)

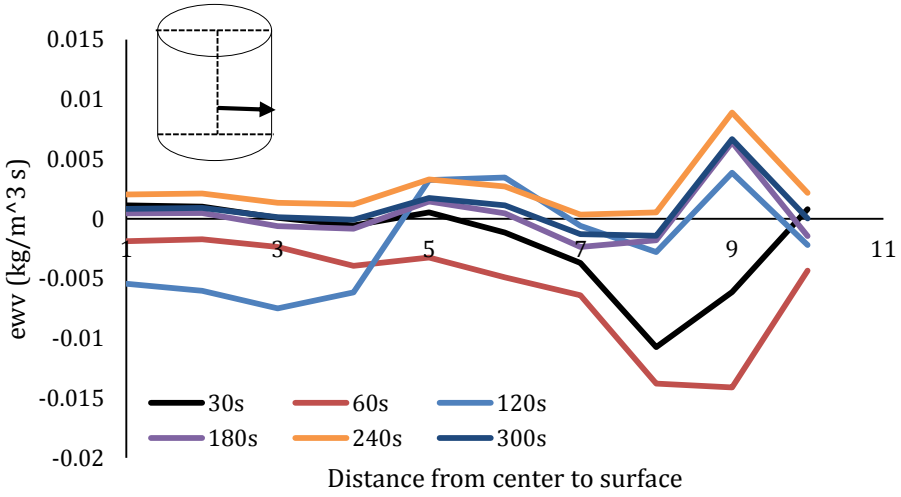

Figure 21c. Spatial distribution of evaporation rate (kg/m^3 s) within apple cylinders (below the center line)

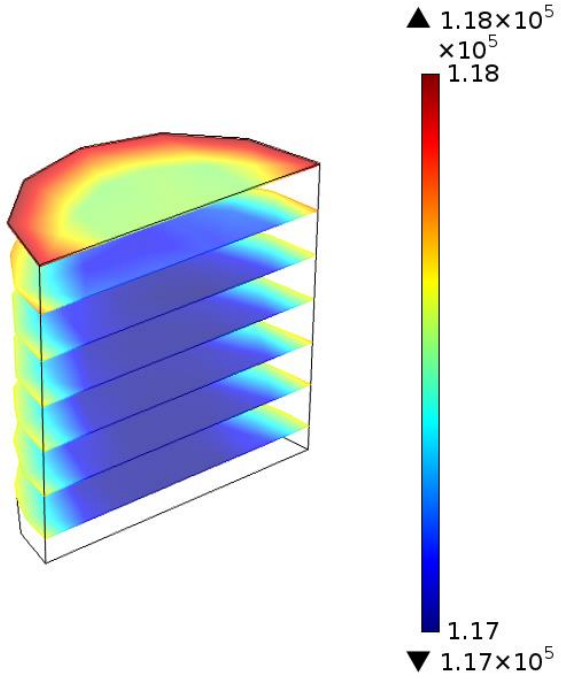

Figure 22a. Slice plots of Young's modulus (Pa) at 30s drying

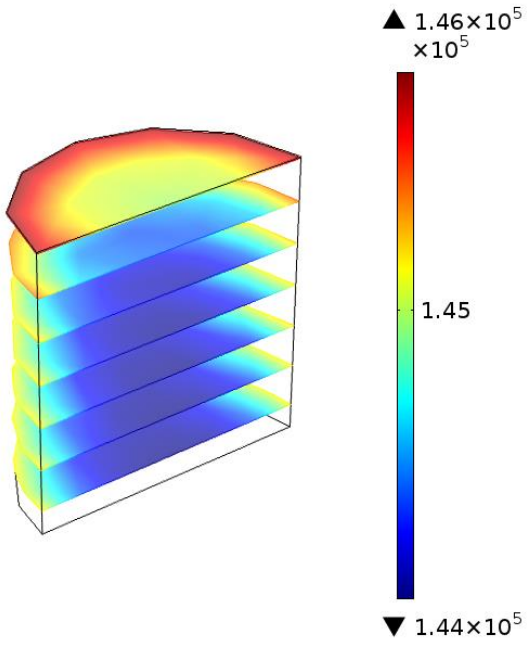

Figure 22b. Slice plots of Young's modulus (Pa) at 60s drying

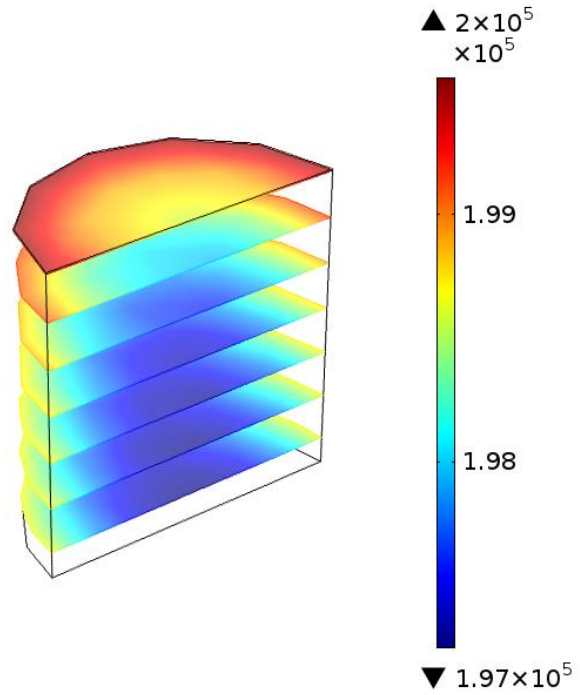

Figure 22c. Slice plots of Young's modulus (Pa) at 120s drying

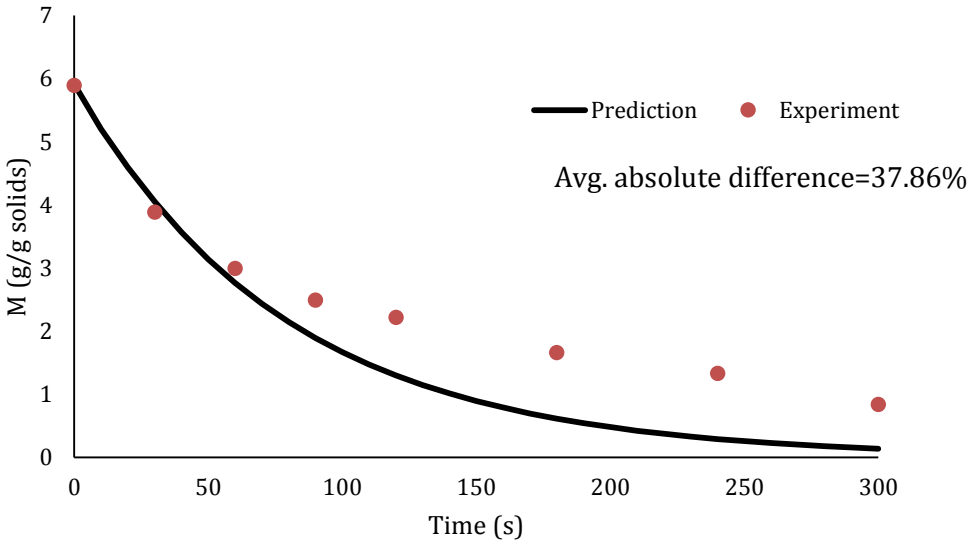

Figure 23a. Volume-averaged moisture content (g/g solids) in sample at $k = 0.4\ W/m \cdot K$

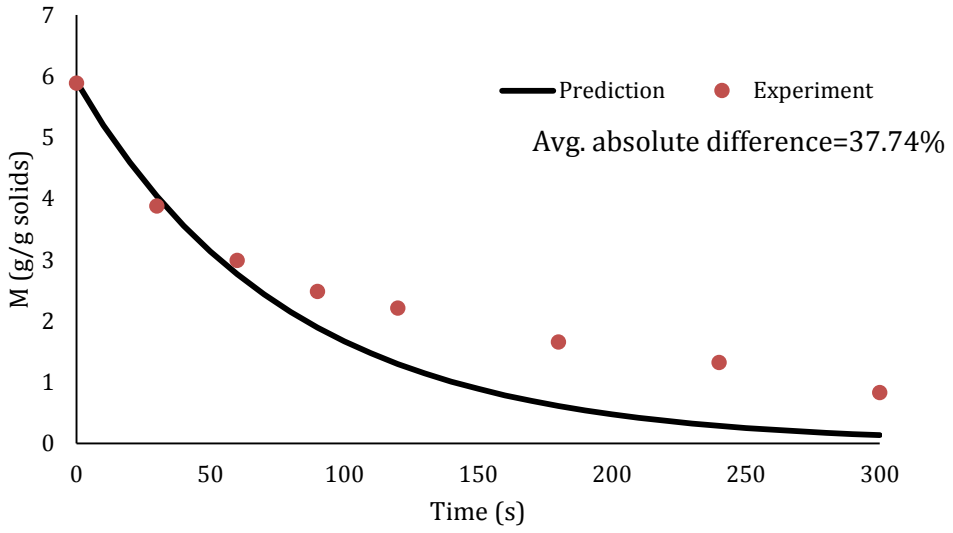

Figure 23b. Volume-averaged moisture content (g/g solids) in sample at $k = 0.5\ W/m \cdot K$

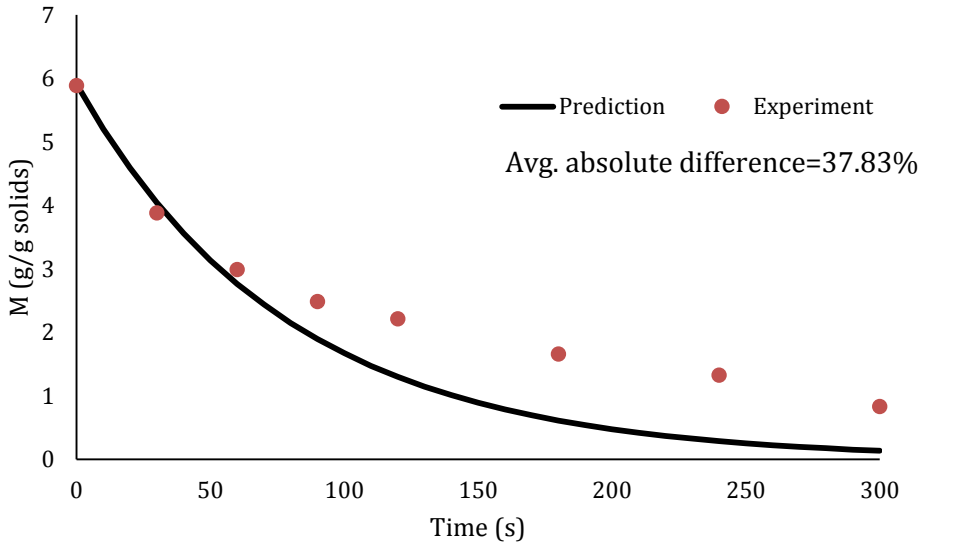

Figure 23c. Volume-averaged moisture content (g/g solids) in sample at $k = 0.6\ W/m \cdot K$

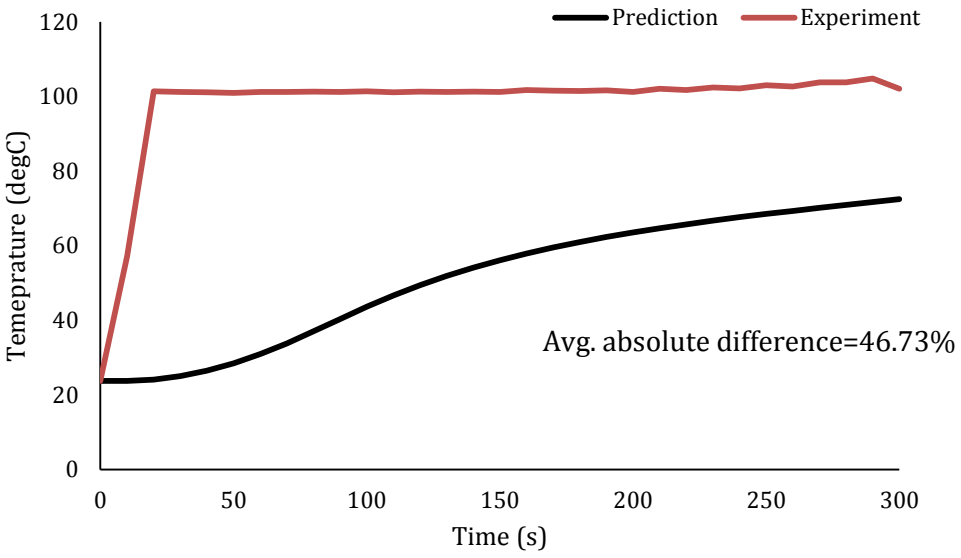

Figure 24a. Line-averaged temperature (°C) in sample at $k = 0.4\ W/m \cdot K$

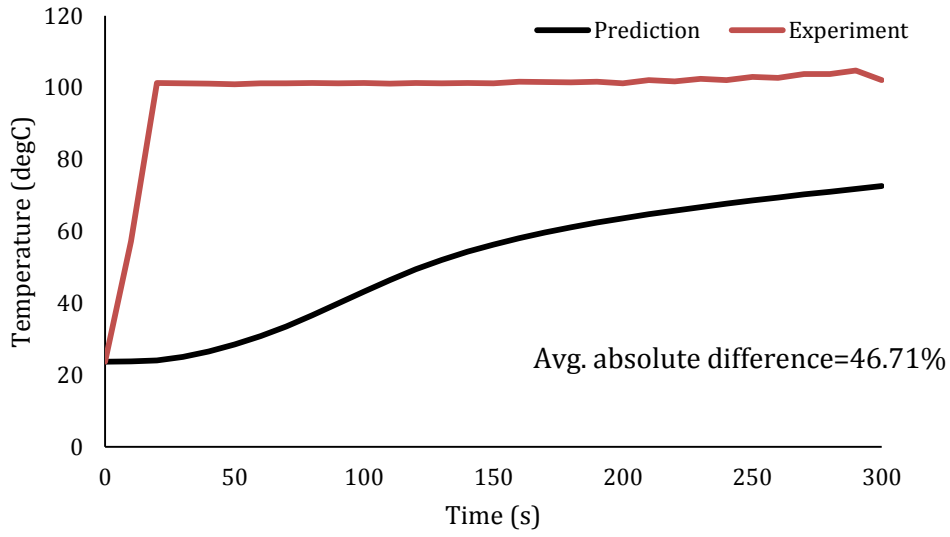

Figure 24b. Line-averaged temperature (°C) in sample at $k = 0.5\ W/m \cdot K$

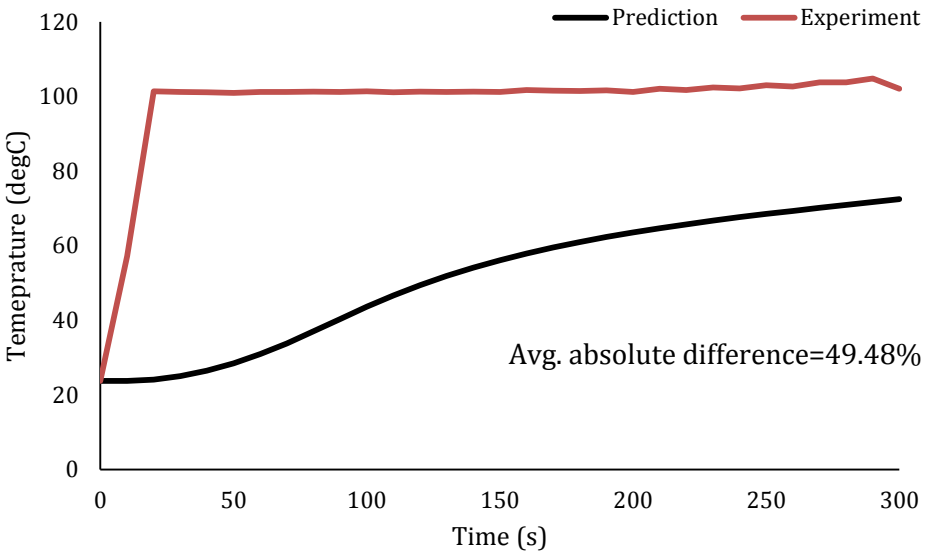

Figure 24c. Line-averaged temperature (°C) in sample at $k = 0.6\ W/m \cdot K$

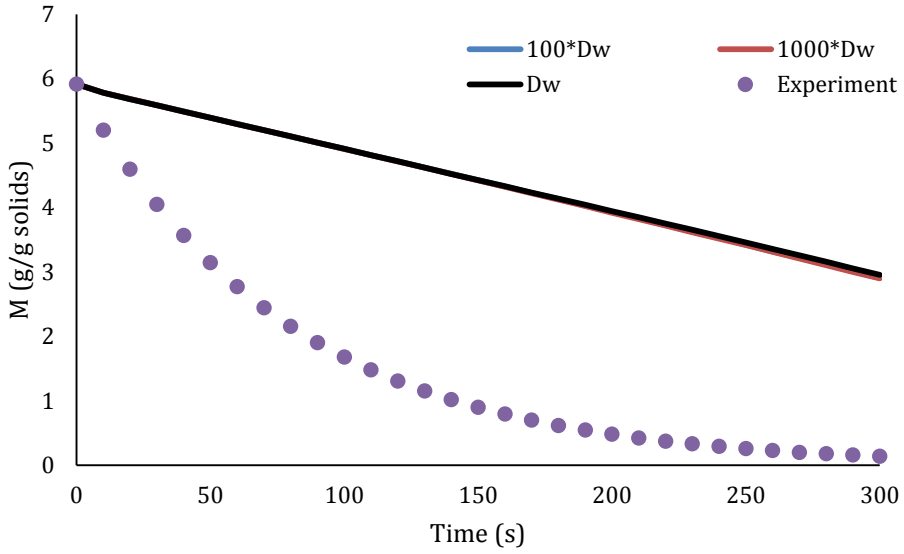

Figure 25. Volume-averaged moisture content (g/g solids) in sample at different diffusivity values

Table 1. Initial and Boundary conditions

Parameter	Value	Unit	Source
Initial volume fraction of water	$\varepsilon_i^w = 0.72$	Dimensionless	Measured with moisture analyzer
Initial volume fraction of gas	$\varepsilon_i^g = 0.01 - 0.05$	Dimensionless	Estimated
Initial vapor density	$\rho_i^v = 0.022$	kg/m^3	Ideal gas law
Porosity	$\phi = \varepsilon^w + \varepsilon^g$	Dimensionless	
Initial temperature	$T_i = 293.15$	K	Measured with thermometer
Initial pressure	$p_i = p_{atm}$ (101325)	Pa	Atmospheric pressure
Initial electric field intensity	$\boldsymbol{E}_i = 0$	V/m	From oven condition
Relative humidity	$R_H = 0.72$	Dimensionless	Measured in room condition
Moisture flux	$Q_w = h_w(p_{veq} - p_a)$	m/s	
Vapor flux	$Q_v = h_v(p_v - p_a)$	m/s	
Energy flux	$h_T(T - T_{amb}) + \varepsilon\sigma_S F_{12}(T^4 - T_{amb}^4)$, where h_T follows Ratti and Crapiste (1994), $F_{12} = 1, \varepsilon = 0.94$		Ratti and Crapiste (1995); Hellebrand et al. (2001)

Table 2. Material properties and supporting relations

Property	Equation or value	Source
Moisture content	$M = \frac{\rho^w \varepsilon^w}{\rho^s (1-\phi)}$ (32)	Takhar (2011)
Water activity	$a_w = 1 - \exp(-1.73e-4(T - 273.15 + 41.9) \cdot (100M)^{1.345})$	ASABE (2007)
Binary diffusivity (m^2/s)	$D_v = -2.775\times10^{-6} + 4.479\times10^{-8}T + 1.656\times10^{-10}T^2$	Nellis & Klein (2008)
Specific heat capacity of solid (J/ kg·K)	$C_{ps} = 10.581(T - 273.15) + 2891.3$	Pakowski & Adamski (2012)
Porosity	$\phi = \frac{1.282 + 1.65(1.89 + M) \cdot M}{(1+1.65M) \cdot (1.899 + M)}$	Krokida & Maroulis (1999)
Thermal conductivity of solid (W/(m°K))	$k_s = 0.201 + 1.39\times10^{-3}(T - 273.15) + 4.33\times10^{-6}(T - 273.15)^2$	Rahman, Chen & Perera (1997)
Water saturation	$S_w = \frac{w}{\phi}$	
Capillary pressure (Pa)	$p_c = 56.75\times10^3(1 - S_w) \cdot \exp(\frac{1.062}{S_w})$	Leverett (1941)
Saturated pressure (Pa)	$p_s = \exp(\frac{-6096.9385}{T} + 21.2409642 - 0.02711193T + 0.1673952\times10^{-4}T^2 + 2.433502\ln(T))$	Perry & Green (2008)
Vapor pressure of water at equilibrium (P_a)	$p_{veq} = a_w p_{sat}$	Takhar (2011)
Partial pressure of air (P_a)	$p_a = R_a \rho_a T_{amb}$ ($R_a = \frac{R}{M_a}$, where M_a is the molecular weight of air)	Ideal gas law

Table2 (cont.)

Partial pressure of vapor(P_a)	$p_v = R_v \rho_v T$ ($R_v = \frac{R}{M_v}$, where M_v is the molecular weight of vapor)	Ideal gas law
Evaporation rate ($kg / m^3 s$)	${}^w\hat{e}^v = 1 \cdot \log(\frac{p_{veq}}{p_v})$	Takhar (2014)
Ambient temperature (K)	$T_{amb} = 0.4256t + 297.15,\ 0<t \le 80$ $T_{amb} = 0.0705t + 327.507,\ t>80$	Measured with temperature sensor